Revised Michaelis–Menten Rate Law with Time-Varying Molecular Concentrations

Roktaek Lim[1,7], Thomas L. P. Martin[1,7], Junghun Chae[2,7], WooJoong Kim[2], Cheol-Min Ghim[2,3,*], and Pan-Jun Kim[1,4,5,6,*]

[1]Department of Biology, Hong Kong Baptist University, Kowloon, Hong Kong
[2]Department of Physics, Ulsan National Institute of Science and Technology, Ulsan 44919, Republic of Korea
[3]Department of Biomedical Engineering, Ulsan National Institute of Science and Technology, Ulsan 44919, Republic of Korea
[4]Center for Quantitative Systems Biology & Institute of Computational and Theoretical Studies, Hong Kong Baptist University, Kowloon, Hong Kong
[5]State Key Laboratory of Environmental and Biological Analysis, Hong Kong Baptist University, Kowloon, Hong Kong
[6]Abdus Salam International Centre for Theoretical Physics, 34151 Trieste, Italy
[7]R.L., T.L.P.M., and J.C. contributed equally to this work.
[*]Author to whom correspondence should be addressed: C.-M.G. (email: cmghim@unist.ac.kr) or P.-J.K. (email: panjunkim@hkbu.edu.hk)

Abstract

Despite over a century's use as a dominant paradigm in the description of biochemical rate processes, the Michaelis–Menten (MM) rate law stands on the restrictive assumption that the concentration of the complex of interacting molecules, at each moment, approaches an equilibrium much faster than the molecular concentration changes. The increasingly-appreciated, remedied form of the MM rate law is also based on this quasi-steady state assumption. Although this assumption may be valid for a range of biochemical systems, the exact extent of such systems is not clear. In this study, we relax the quasi-steady state requirement and propose the revised MM rate law for the interactions of molecules with active concentration changes over time. Our revised rate law, characterized by rigorously-derived time delay effects in molecular complex formation, improves the accuracy of models especially for protein–protein and protein–DNA interactions. Our simulation and empirical data analysis show that the improvement is not limited to the quantitatively better characterization of dynamics such as the signal response of autogenously regulated systems, and allows the prediction for qualitatively new patterns. The latter involves the oscillation condition and period patterns of the mammalian circadian clock and the spontaneous rhythmicity in the degradation rates of circadian proteins, both not properly captured by the previous approaches. Moreover, our revised rate law allows more accurate parameter estimation. This work offers an analytical framework for understanding rich transient or rhythmic dynamics of biomolecular systems, which goes beyond the quasi-steady state assumption.

I. INTRODUCTION

Since proposed by Henri [1] and Michaelis and Menten [2], the Michaelis–Menten (MM) rate law has been the dominant framework for modeling the rates of enzyme-catalyzed reactions for over a century [1–4]. The MM rate law has also been widely adopted for describing other bimolecular interactions, such as reversible binding between proteins [5–7], between a gene and a transcription factor (TF) [8,9], and between a receptor and a ligand [10,11]. The derivation of the MM rate law from the underlying biochemical mechanism is based on the steady-state approximation by Briggs and Haldane [3], referred to as the *standard quasi-steady state approximation* (sQSSA) [12–14]. The sQSSA, however, is only valid when the enzyme concentration is low enough and thus the concentration of enzyme–substrate complex is negligible compared to substrate concentration [14]. This condition may be acceptable for many metabolic reactions with substrate concentrations that are typically far higher than the enzyme concentrations.

Nevertheless, in the case of protein–protein interactions in various cellular activities, the interacting proteins as the "enzymes" and "substrates" often show the concentrations comparable with each other [15–17]. Therefore, the use of the MM rate law for describing protein–protein interactions has been challenged in its rationale, with the modified alternative formula from the *total quasi-steady state approximation* (tQSSA) [12,13,18–24]. The tQSSA-based form is generally more accurate than the MM rate law from the sQSSA, for a broad range of combined molecular concentrations and thus for protein–protein interactions as well [12,13,18–24]. The superiority of the tQSSA has not only been proven in the quantitative, but also in the qualitative outcomes of systems, which the sQSSA sometimes fails to predict [12,18]. Later, we will provide the overview of the tQSSA and its relationship with the conventional MM rate law from the sQSSA.

Despite the correction of the MM rate law by the tQSSA, both the tQSSA and sQSSA still rely on the assumption that the concentration of the complex of interacting molecules, at each moment, approaches an equilibrium much faster than the molecular concentration changes [12,14,21]. Although this quasi-steady state assumption may work for a range of biochemical systems, the exact extent of such systems to follow that assumption is not clear. Numerous cellular processes do exhibit active molecular concentration changes over time, such as in circadian clock circuits or cell cycle systems [6,7,18,25–28], calling for a better approach to even cover the time-varying molecular concentrations that may not strictly adhere to the quasi-steady state assumption.

In this study, we report the revision of the MM rate law, whereby the interaction of time-varying molecular components is more precisely described than by the existing approaches including the tQSSA. This revision is the correction of the tQSSA with rigorously-estimated time-delay effects, which improves the predictability for quantitative molecular-binding kinetics and retrieves the tQSSA in steady conditions. Our formulation well accounts for the transient or oscillatory dynamics and empirical patterns of biomolecular systems with the relevant analytical insights, which are not captured by the previous methods—the tQSSA and sQSSA. This work offers a new mathematical framework for interrogating rich dynamics of molecular interactions in a broad range of biochemical contexts.

II. THEORY OVERVIEW AND DERIVATION

A. General formulation

We consider two different molecules A and B that bind to each other and form complex AB. For example, A and B may represent two participant proteins in heterodimer formation, a chemical substrate and an enzyme in a metabolic reaction, and a solute and a transporter in

membrane transport. The concentration of the complex AB at time t, denoted by $C(t)$, changes over time as in the following equation:

$$\frac{\mathrm{d}C(t)}{\mathrm{d}t} = k_{\mathrm{a}}[A(t) - C(t)][B(t) - C(t)] - k_{\delta}C(t). \qquad (1)$$

Here, $A(t)$ and $B(t)$ denote the total concentrations of A and B, respectively, and hence $A(t) - C(t)$ and $B(t) - C(t)$ correspond to the concentrations of free A and B. k_{a} denotes the association rate of free A and B. k_{δ} is defined as $k_{\delta} \equiv k_{\mathrm{d}} + r_{\mathrm{c}} + k_{\mathrm{loc}} + k_{\mathrm{dlt}}$ where k_{d}, k_{loc}, and k_{dlt} stand for the dissociation, translocation, and dilution rates of AB, respectively, and r_{c} for the chemical conversion or translocation rate of A or B upon the formation of AB.

Using the notations $\tau \equiv k_{\delta}t$, $K \equiv k_{\delta}/k_{\mathrm{a}}$, $\bar{A}(\tau) \equiv A(t)/K$, $\bar{B}(\tau) \equiv B(t)/K$, and $\bar{C}(\tau) \equiv C(t)/K$, one can rewrite Eq. (1) as

$$\frac{\mathrm{d}\bar{C}(\tau)}{\mathrm{d}\tau} = [\bar{A}(\tau) - \bar{C}(\tau)][\bar{B}(\tau) - \bar{C}(\tau)] - \bar{C}(\tau). \qquad (2)$$

By definition, $C(t) \leq A(t)$ and $C(t) \leq B(t)$, and therefore

$$C(t) \leq \min[A(t), B(t)] \text{ \{i.e., } \overline{C}(\tau) \leq \min\left[\overline{A}(\tau), \overline{B}(\tau)\right]\text{\}}. \qquad (3)$$

On the other hand, Eq. (2) is equivalent to

$$\frac{\mathrm{d}\bar{C}(\tau)}{\mathrm{d}\tau} = \left[\bar{C}(\tau) - \bar{C}_{\mathrm{tQ}}(\tau)\right]\left\{\bar{C}(\tau) - \left[\bar{C}_{\mathrm{tQ}}(\tau) + \sqrt{\Delta_{\mathrm{tQ}}(\tau)}\right]\right\}, \qquad (4)$$

where $\bar{C}_{\mathrm{tQ}}(\tau)$ and $\Delta_{\mathrm{tQ}}(\tau)$ are given by

$$\bar{C}_{\mathrm{tQ}}(\tau) \equiv \frac{1}{2}\left[1 + \overline{A}(\tau) + \overline{B}(\tau) - \sqrt{\Delta_{\mathrm{tQ}}(\tau)}\right], \qquad (5)$$

$$\begin{aligned}\Delta_{\mathrm{tQ}}(\tau) &\equiv [1 + \overline{A}(\tau) + \overline{B}(\tau)]^2 - 4\overline{A}(\tau)\overline{B}(\tau) \\ &= 1 + 2\left[\overline{A}(\tau) + \overline{B}(\tau)\right] + [\overline{A}(\tau) - \overline{B}(\tau)]^2. \qquad (6)\end{aligned}$$

In the tQSSA, the assumption is that $C(t)$ approaches the equilibrium fast enough each time, given the values of $A(t)$ and $B(t)$ [12,21]. To understand this idea, notice that $\bar{C}'(\tau) \to 0$ in Eq. (4) when $\bar{C}(\tau) \to \bar{C}_{\mathrm{tQ}}(\tau)$ given the values of $\overline{A}(\tau)$ and $\overline{B}(\tau)$ [we use symbol ' for a derivative, such as $\bar{C}'(\tau)$ here]. One can prove that $\bar{C}_{\mathrm{tQ}}(\tau) \leq \min\left[\overline{A}(\tau), \overline{B}(\tau)\right]$ and thus Eq. (3) is naturally satisfied when $\bar{C}(\tau) = \bar{C}_{\mathrm{tQ}}(\tau)$. The other nominal solution of $\bar{C}'(\tau) = 0$ in Eq. (4) does not satisfy Eq. (3) and is thus physically senseless.

According to the tQSSA, one takes an estimate $\bar{C}(\tau) \approx \bar{C}_{\mathrm{tQ}}(\tau)$, or equivalently, $C(t) \approx C_{\mathrm{tQ}}(t)$ with this form:

$$C_{\mathrm{tQ}}(t) \equiv \frac{1}{2}\left\{K + A(t) + B(t) - \sqrt{[K + A(t) + B(t)]^2 - 4A(t)B(t)}\right\}. \qquad (7)$$

As mentioned earlier, the tQSSA is generally more accurate than the conventional MM rate law [12,13,18–24]. To obtain the MM rate law, consider a rather specific condition,

$$B(t) \ll K + A(t) \text{ or } A(t) \ll K + B(t) \text{ [i.e., } \overline{B}(\tau) \ll 1 + \overline{A}(\tau) \text{ or } \overline{A}(\tau) \ll 1 + \overline{B}(\tau)\text{]}. \qquad (8)$$

In this condition, the Padé approximant for $C_{\mathrm{tQ}}(t)$ takes the following form:

$$C_{\mathrm{tQ}}(t) \approx \frac{A(t)B(t)}{K + A(t) + B(t)} \text{ [i.e., } \bar{C}_{\mathrm{tQ}}(\tau) \approx \frac{\overline{A}(\tau)\overline{B}(\tau)}{1 + \overline{A}(\tau) + \overline{B}(\tau)}\text{]}. \qquad (9)$$

Considering Eq. (9), Eq. (8) is similar to the condition $C_{\mathrm{tQ}}(t)/A(t) \ll 1$ or $C_{\mathrm{tQ}}(t)/B(t) \ll 1$. In other words, Eq. (9) would be valid when the concentration of AB complex is negligible compared to either A or B's concentration. This condition is essentially identical to the assumption in the sQSSA resulting in the MM rate law [14]. In the example of a typical metabolic reaction with $B(t) \ll A(t)$ for substrate A and enzyme B, Eq. (8) is automatically satisfied and Eq. (9) further reduces to the familiar MM rate law $C_{\mathrm{tQ}}(t) \approx A(t)B(t)/[K + A(t)]$, the outcome of the sQSSA [1–4,12–14]. To be precise, the sQSSA uses the concentration of free A instead of $A(t)$, but we refer to this formula with $A(t)$ as the sQSSA because the complex is assumed to be negligible in that scheme. Clearly, K here is the Michaelis constant, commonly known as K_{M}.

The application of the MM rate law beyond the condition in Eq. (8) invites a risk of erroneous modeling results, whereas the tQSSA is relatively free of such errors and has wider applicability [12,13,18–24]. Still, both the tQSSA and sQSSA stand on the quasi-steady state assumption that $C(t)$ approaches the equilibrium fast enough each time before the marked temporal

change of $A(t)$ or $B(t)$. Next, we will relieve this assumption and improve the approximation of $C(t)$ in the case of time-varying $A(t)$ and $B(t)$, as the main objective of this study.

Suppose that $C(t)$ may not necessarily approach the equilibrium $C_{\mathrm{tQ}}(t)$ but stays within some distance from it, satisfying the following relation:

$$\left|\bar{C}(\tau)-\bar{C}_{\mathrm{tQ}}(\tau)\right| \ll \sqrt{\Delta_{\mathrm{tQ}}(\tau)}. \qquad (10)$$

We will later show that this relation is readily satisfied in physiologically-relevant conditions. This relation allows us to discard $\left[\bar{C}(\tau)-\bar{C}_{\mathrm{tQ}}(\tau)\right]^2$ compared to $\sqrt{\Delta_{\mathrm{tQ}}(\tau)}\left[\bar{C}(\tau)-\bar{C}_{\mathrm{tQ}}(\tau)\right]$ and thereby reduce Eq. (4) to

$$\frac{\mathrm{d}\bar{C}(\tau)}{\mathrm{d}\tau} \approx \sqrt{\Delta_{\mathrm{tQ}}(\tau)}\left[\bar{C}_{\mathrm{tQ}}(\tau)-\bar{C}(\tau)\right]. \qquad (11)$$

The solution of Eq. (11) is given by

$$\bar{C}(\tau) \approx \int_{\tau_0}^{\tau}\sqrt{\Delta_{\mathrm{tQ}}(\tau')}\bar{C}_{\mathrm{tQ}}(\tau')e^{-\int_{\tau'}^{\tau}\sqrt{\Delta_{\mathrm{tQ}}(\tau'')}\mathrm{d}\tau''}\mathrm{d}\tau' + \bar{C}(\tau_0)e^{-\int_{\tau_0}^{\tau}\sqrt{\Delta_{\mathrm{tQ}}(\tau')}\mathrm{d}\tau'}, \qquad (12)$$

where τ_0 denotes an arbitrarily assigned, initial point of τ. Assume that $\sqrt{\Delta_{\mathrm{tQ}}(\tau')}$ changes rather slowly over τ' to satisfy

$$\sqrt{\Delta_{\mathrm{tQ}}(\tau')} \approx \sqrt{\Delta_{\mathrm{tQ}}(\tau)} \text{ for } \tau' \text{ in the range } \tau-\frac{1}{\sqrt{\Delta_{\mathrm{tQ}}(\tau)}} \lesssim \tau' \leq \tau. \qquad (13)$$

As we will show later, Eq. (13) is satisfied as readily as Eq. (10) in physiologically-relevant conditions. With Eq. (13), Eq. (12) for $\tau \gg \tau_0 + \Delta_{\mathrm{tQ}}^{-1/2}(\tau_0)$ is further approximated as

$$\bar{C}(\tau) \approx \sqrt{\Delta_{\mathrm{tQ}}(\tau)}\int_{-\infty}^{\tau}\bar{C}_{\mathrm{tQ}}(\tau')e^{-\sqrt{\Delta_{\mathrm{tQ}}(\tau)}(\tau-\tau')}\mathrm{d}\tau'. \qquad (14)$$

The Taylor expansion $\bar{C}_{\mathrm{tQ}}(\tau') = \bar{C}_{\mathrm{tQ}}(\tau) - (\tau-\tau')\bar{C}'_{\mathrm{tQ}}(\tau) + (\tau-\tau')^2\bar{C}''_{\mathrm{tQ}}(\tau)/2 - \cdots$ leads Eq. (14) to

$$\begin{aligned}\bar{C}(\tau) &\approx \bar{C}_{\mathrm{tQ}}(\tau) - \frac{1}{\sqrt{\Delta_{\mathrm{tQ}}(\tau)}}\frac{\mathrm{d}\bar{C}_{\mathrm{tQ}}(\tau)}{\mathrm{d}\tau}\int_0^{\infty}xe^{-x}\mathrm{d}x + \frac{1}{2\Delta_{\mathrm{tQ}}(\tau)}\frac{\mathrm{d}^2\bar{C}_{\mathrm{tQ}}(\tau)}{\mathrm{d}\tau^2}\int_0^{\infty}x^2e^{-x}\mathrm{d}x - \cdots \\ &= \bar{C}_{\mathrm{tQ}}(\tau) - \frac{1}{\sqrt{\Delta_{\mathrm{tQ}}(\tau)}}\frac{\mathrm{d}\bar{C}_{\mathrm{tQ}}(\tau)}{\mathrm{d}\tau} + \frac{1}{\Delta_{\mathrm{tQ}}(\tau)}\frac{\mathrm{d}^2\bar{C}_{\mathrm{tQ}}(\tau)}{\mathrm{d}\tau^2} - \cdots \\ &= \bar{C}_{\mathrm{tQe}}(\tau) + \frac{1}{\Delta_{\mathrm{tQ}}(\tau)}\frac{\mathrm{d}^2\bar{C}_{\mathrm{tQ}}(\tau)}{\mathrm{d}\tau^2} - \cdots, \qquad (15)\end{aligned}$$

where $\bar{C}_{\mathrm{tQe}}(\tau)$ is defined as

$$\bar{C}_{\mathrm{tQe}}(\tau) \equiv \bar{C}_{\mathrm{tQ}}(\tau) - \frac{1}{\sqrt{\Delta_{\mathrm{tQ}}(\tau)}}\frac{\mathrm{d}\bar{C}_{\mathrm{tQ}}(\tau)}{\mathrm{d}\tau}. \qquad (16)$$

For the approximation of $\bar{C}(\tau)$, one may be tempted to use $\bar{C}_{\mathrm{tQe}}(\tau)$ in Eq. (16). However, as proven in Text S1, the sheer use of $\bar{C}_{\mathrm{tQe}}(\tau)$ is susceptible to the overestimation of the amplitude of $\bar{C}(\tau)$ when $\bar{C}(\tau)$ is rhythmic over time. To detour this overestimation problem, we take the Taylor expansion of the time-delayed form of $\bar{C}_{\mathrm{tQ}}(\tau)$:

$$\bar{C}_{\mathrm{tQ}}\left[\tau - \frac{1}{\sqrt{\Delta_{\mathrm{tQ}}(\tau)}}\right] = \bar{C}_{\mathrm{tQ}}(\tau) - \frac{1}{\sqrt{\Delta_{\mathrm{tQ}}(\tau)}}\frac{\mathrm{d}\bar{C}_{\mathrm{tQ}}(\tau)}{\mathrm{d}\tau} + \frac{1}{2\Delta_{\mathrm{tQ}}(\tau)}\frac{\mathrm{d}^2\bar{C}_{\mathrm{tQ}}(\tau)}{\mathrm{d}\tau^2} - \cdots. \qquad (17)$$

Strikingly, the zeroth-order and first-order derivative terms of $\bar{C}_{\mathrm{tQ}}(\tau)$ on the right-hand side above are identical to $\bar{C}_{\mathrm{tQe}}(\tau)$, and the second-order derivative term still covers a half of that term in Eq. (15). Hence, $\bar{C}_{\mathrm{tQ}}\left[\tau - \Delta_{\mathrm{tQ}}^{-1/2}(\tau)\right]$ and correspondingly, $C_{\mathrm{tQ}}\left[t - k_{\delta}^{-1}\Delta_{\mathrm{tQ}}^{-1/2}(t)\right]$ bear the potential for the approximants of $\bar{C}(\tau)$ and $C(t)$, respectively. Besides, the overestimation of the amplitude of rhythmic $\bar{C}(\tau)$ by $\bar{C}_{\mathrm{tQ}}\left[\tau - \Delta_{\mathrm{tQ}}^{-1/2}(\tau)\right]$ would not be as serious as by $\bar{C}_{\mathrm{tQe}}(\tau)$ and at worst equals that by $\bar{C}_{\mathrm{tQ}}(\tau)$ (Text S1), because $\bar{C}_{\mathrm{tQ}}\left[\tau - \Delta_{\mathrm{tQ}}^{-1/2}(\tau)\right]$ and $\bar{C}_{\mathrm{tQ}}(\tau)$ themselves have the same amplitudes.

The distinct feature of $\bar{C}_{\mathrm{tQ}}\left[\tau-\Delta_{\mathrm{tQ}}^{-1/2}(\tau)\right]$ or equivalent $C_{\mathrm{tQ}}\left[t-k_{\delta}^{-1}\Delta_{\mathrm{tQ}}^{-1/2}(t)\right]$ is the inclusion of an effective time delay $k_{\delta}^{-1}\Delta_{\mathrm{tQ}}^{-1/2}(t)$ in the formation of AB complex. As we will address later, this feature helps to capture intriguing biomolecular dynamics with time-varying molecular concentrations, which is not covered by the tQSSA. The effective time delay $k_{\delta}^{-1}\Delta_{\mathrm{tQ}}^{-1/2}(t)$ becomes prominent for small k_{δ} and for unsaturated molecules A and B with comparable concentrations—i.e., with small $\overline{A}(\tau)+\overline{B}(\tau)$ and $[\overline{A}(\tau)-\overline{B}(\tau)]^2$ in Eq. (6). In other words, in the opposite limit, the time delay becomes short and then $\bar{C}_{\mathrm{tQ}}\left[\tau-\Delta_{\mathrm{tQ}}^{-1/2}(\tau)\right]$ converges to $\bar{C}_{\mathrm{tQ}}(\tau)$, the tQSSA.

One caveat with the use of $\bar{C}_{\mathrm{tQ}}\left[\tau-\Delta_{\mathrm{tQ}}^{-1/2}(\tau)\right]$ to estimate $\bar{C}(\tau)$ is that $\bar{C}_{\mathrm{tQ}}\left[\tau-\Delta_{\mathrm{tQ}}^{-1/2}(\tau)\right]$ may not necessarily satisfy the relation $\bar{C}_{\mathrm{tQ}}\left[\tau-\Delta_{\mathrm{tQ}}^{-1/2}(\tau)\right]\leq\min\left[\overline{A}(\tau),\overline{B}(\tau)\right]$ favored by Eq. (3). As a practical safeguard to avoid this problem, we propose the following approximant for $\bar{C}(\tau)$ consistent with Eq. (3):

$$\bar{C}_{\gamma}(\tau)\equiv\min\left\{\bar{C}_{\mathrm{tQ}}\left[\tau-\Delta_{\mathrm{tQ}}^{-1/2}(\tau)\right],\bar{A}(\tau),\bar{B}(\tau)\right\}. \qquad (18)$$

The corresponding approximant for $C(t)$ is

$$C_{\gamma}(t)\equiv\min\left\{C_{\mathrm{tQ}}\left[t-k_{\delta}^{-1}\Delta_{\mathrm{tQ}}^{-1/2}(t)\right],A(t),B(t)\right\}. \qquad (19)$$

As will be demonstrated later, the accuracy of this approximation [$\bar{C}_{\gamma}(\tau)$ or $C_{\gamma}(t)$] surpasses that of the tQSSA [$\bar{C}_{\mathrm{tQ}}(\tau)$ or $C_{\mathrm{tQ}}(t)$]. In the case where Eq. (8) is satisfied, $\bar{C}_{\mathrm{tQ}}\left[\tau-\Delta_{\mathrm{tQ}}^{-1/2}(\tau)\right]$ and $C_{\mathrm{tQ}}\left[t-k_{\delta}^{-1}\Delta_{\mathrm{tQ}}^{-1/2}(t)\right]$ in Eqs. (18) and (19) can be further approximated by the MM-like forms in Eq. (9) with the time-delay terms $\Delta_{\mathrm{tQ}}^{-1/2}(\tau)\approx 1/\left[1+\overline{A}(\tau)+\overline{B}(\tau)\right]$ and $k_{\delta}^{-1}\Delta_{\mathrm{tQ}}^{-1/2}(t)\approx k_{\delta}^{-1}K/[K+A(t)+B(t)]$. On the other hand, Eqs. (18) and (19) are ill-defined for $\tau-\Delta_{\mathrm{tQ}}^{-1/2}(\tau)<\tau_0$ where τ_0 is an initial point of τ. In fact, from the last term in Eq. (12), τ should satisfy $\tau\gg\tau_0+\Delta_{\mathrm{tQ}}^{-1/2}(\tau_0)$ for the application of any rate law [e.g., Eq. (18) or (19), the tQSSA, and the sQSSA] whose form does not depend on the initial conditions.

One may question the analytical utility of $\bar{C}_{\gamma}(\tau)$ and $C_{\gamma}(t)$ in Eqs. (18) and (19), regarding the apparent complexity of their mathematical structure. In Secs. III.D and III.F, our approach with simpler forms will be used to deliver valuable analytical insights into the systems whose dynamics is otherwise ill-described by the conventional tQSSA and sQSSA.

To clarify the preconditions for the use of our approximation, we first revisit the condition in Eq. (10). Replacing $\bar{C}(\tau)$ in Eq. (10) by $\bar{C}_{\mathrm{tQe}}(\tau)$ in Eqs. (15) and (16) leads to the following self-consistency condition:

$$\varepsilon_1(\tau)\equiv\frac{1}{\Delta_{\mathrm{tQ}}(\tau)}\left|\frac{\mathrm{d}\bar{C}_{\mathrm{tQ}}(\tau)}{\mathrm{d}\tau}\right|\ll 1, \qquad (20)$$

where $\bar{C}'_{\mathrm{tQ}}(\tau)$ is given by

$$\frac{\mathrm{d}\bar{C}_{\mathrm{tQ}}(\tau)}{\mathrm{d}\tau}=\frac{1}{\sqrt{\Delta_{\mathrm{tQ}}(\tau)}}\left\{\left[\bar{B}(\tau)-\bar{C}_{\mathrm{tQ}}(\tau)\right]\bar{A}(\tau)\mu_{\mathrm{A}}(\tau)+\left[\bar{A}(\tau)-\bar{C}_{\mathrm{tQ}}(\tau)\right]\bar{B}(\tau)\mu_{\mathrm{B}}(\tau)\right\}. \qquad (21)$$

Here, $\mu_{\mathrm{A}}(\tau)\equiv\bar{A}'(\tau)/\bar{A}(\tau)$, $\mu_{\mathrm{B}}(\tau)\equiv\bar{B}'(\tau)/\bar{B}(\tau)$, and the derivation of Eq. (21) is straightforward from Eq. (5). For the sake of simplicity, we will keep using these notations $\mu_{\mathrm{A}}(\tau)$ and $\mu_{\mathrm{B}}(\tau)$ throughout this work. Next, we revisit another condition in Eq. (13). By applying $\sqrt{\Delta_{\mathrm{tQ}}(\tau')}\approx\sqrt{\Delta_{\mathrm{tQ}}(\tau)}+(\tau'-\tau)\left[\sqrt{\Delta_{\mathrm{tQ}}(\tau)}\right]'$ to Eq. (13), we obtain $\Delta_{\mathrm{tQ}}^{-1}(\tau)\left[\sqrt{\Delta_{\mathrm{tQ}}(\tau)}\right]'\ll 1$. By the definition of $\Delta_{\mathrm{tQ}}(\tau)$ in Eq. (6), this condition is equivalent to

$$\varepsilon_2(\tau)\equiv\Delta_{\mathrm{tQ}}^{-\frac{3}{2}}(\tau)\left|[1+\bar{A}(\tau)-\bar{B}(\tau)]\bar{A}(\tau)\mu_{\mathrm{A}}(\tau)+[1+\bar{B}(\tau)-\bar{A}(\tau)]\bar{B}(\tau)\mu_{\mathrm{B}}(\tau)\right|\ll 1. \qquad (22)$$

The last condition below arises from the comparison between Eqs. (15) and (17), which show the difference of $\sim\Delta_{\mathrm{tQ}}^{-1}(\tau)\bar{C}''_{\mathrm{tQ}}(\tau)/2$:

$$\varepsilon_\gamma(\tau) \equiv \frac{1}{2\Delta_{\mathrm{tQ}}(\tau)\bar{C}_{\mathrm{tQ}}\left[\tau-\Delta_{\mathrm{tQ}}^{-1/2}(\tau)\right]}\left|\frac{\mathrm{d}^2\bar{C}_{\mathrm{tQ}}(\tau)}{\mathrm{d}\tau^2}\right| \ll 1, \quad (23)$$

where $\bar{C}''_{\mathrm{tQ}}(\tau)$ is obtained from Eq. (21) as

$$\begin{aligned}\frac{\mathrm{d}^2\bar{C}_{\mathrm{tQ}}(\tau)}{\mathrm{d}\tau^2} = \Delta_{\mathrm{tQ}}^{-\frac{3}{2}}(\tau)\Big\{&\{\Delta_{\mathrm{tQ}}(\tau) - 2\bar{A}(\tau)[1+\bar{A}(\tau)-\bar{C}_{\mathrm{tQ}}(\tau)]\}[\bar{B}(\tau)-\bar{C}_{\mathrm{tQ}}(\tau)]\bar{A}(\tau)\mu_{\mathrm{A}}^2(\tau) + \\ &\{\Delta_{\mathrm{tQ}}(\tau) - 2\bar{B}(\tau)[1+\bar{B}(\tau)-\bar{C}_{\mathrm{tQ}}(\tau)]\}[\bar{A}(\tau)-\bar{C}_{\mathrm{tQ}}(\tau)]\bar{B}(\tau)\mu_{\mathrm{B}}^2(\tau) + \{1+\Delta_{\mathrm{tQ}}(\tau) - \\ &[\bar{A}(\tau)-\bar{B}(\tau)]^2\}\bar{A}(\tau)\bar{B}(\tau)\mu_{\mathrm{A}}(\tau)\mu_{\mathrm{B}}(\tau) + \Delta_{\mathrm{tQ}}(\tau)\Big\{[\bar{B}(\tau)-\bar{C}_{\mathrm{tQ}}(\tau)]\bar{A}(\tau)\frac{\mathrm{d}\mu_{\mathrm{A}}(\tau)}{\mathrm{d}\tau} + \\ &[\bar{A}(\tau)-\bar{C}_{\mathrm{tQ}}(\tau)]\bar{B}(\tau)\frac{\mathrm{d}\mu_{\mathrm{B}}(\tau)}{\mathrm{d}\tau}\Big\}\Big\}. \quad (24)\end{aligned}$$

In summary, our approximant $\bar{C}_\gamma(\tau)$ shall work when Eqs. (20), (22), and (23) are satisfied. As we will show later, Eqs. (20) and (22) are in fact easy to satisfy and thus only Eq. (23) tends to serve as the relevant factor of the validity of $\bar{C}_\gamma(\tau)$.

On the other hand, the tQSSA would be valid in the following condition from Eq. (15), instead of the condition in Eq. (23):

$$\varepsilon_{\mathrm{tQ}}(\tau) \equiv \frac{1}{\bar{C}_{\mathrm{tQ}}(\tau)}\left|\frac{1}{\sqrt{\Delta_{\mathrm{tQ}}(\tau)}}\frac{\mathrm{d}\bar{C}_{\mathrm{tQ}}(\tau)}{\mathrm{d}\tau} - \frac{1}{\Delta_{\mathrm{tQ}}(\tau)}\frac{\mathrm{d}^2\bar{C}_{\mathrm{tQ}}(\tau)}{\mathrm{d}\tau^2}\right| \ll 1, \quad (25)$$

where $\bar{C}'_{\mathrm{tQ}}(\tau)$ and $\bar{C}''_{\mathrm{tQ}}(\tau)$ are given by Eqs. (21) and (24), respectively. Note that this condition for the tQSSA is more rigorous than the previously-reported condition [21].

Although not mainly deployed in this study, we can even derive a more exact form of $\bar{C}(\tau)$ than $\bar{C}_\gamma(\tau)$ in a certain scenario. We apply the inverse Fourier transform $\bar{C}_{\mathrm{tQ}}(\tau) = \int_{-\infty}^{\infty}\bar{C}_{\mathrm{tQ}}^{\mathrm{f}}(\xi)e^{2\pi i\tau\xi}\mathrm{d}\xi$ to Eq. (14) and then obtain

$$\begin{aligned}\bar{C}(\tau) &\approx \sqrt{\Delta_{\mathrm{tQ}}(\tau)}e^{-\sqrt{\Delta_{\mathrm{tQ}}(\tau)}\tau}\int_{-\infty}^{\infty}\int_{-\infty}^{\tau}\bar{C}_{\mathrm{tQ}}^{\mathrm{f}}(\xi)e^{\left[2\pi i\xi+\sqrt{\Delta_{\mathrm{tQ}}(\tau)}\right]\tau'}\mathrm{d}\tau'\mathrm{d}\xi \\ &= \int_{-\infty}^{\infty}\frac{\bar{C}_{\mathrm{tQ}}^{\mathrm{f}}(\xi)}{\sqrt{1+4\pi^2\Delta_{\mathrm{tQ}}^{-1}(\tau)\xi^2}}e^{i\left\{2\pi\tau\xi-\arctan\left[2\pi\xi\Delta_{\mathrm{tQ}}^{-1/2}(\tau)\right]\right\}}\mathrm{d}\xi \\ &\approx \int_{-\infty}^{\infty}\frac{\bar{C}_{\mathrm{tQ}}^{\mathrm{f}}(\xi)}{\sqrt{1+4\pi^2\Delta_{\mathrm{tQ}}^{-1}(\tau)\xi^2}}e^{2\pi i\xi\left[\tau-\Delta_{\mathrm{tQ}}^{-1/2}(\tau)\right]}\mathrm{d}\xi, \quad (26)\end{aligned}$$

where the last step takes $\arctan(x) \approx x$ for $|x| \ll 1$. Because $\bar{C}_{\mathrm{tQ}}^{\mathrm{f}}(\xi)$ is the Fourier transform of $\bar{C}_{\mathrm{tQ}}(\tau)$, the above result resembles $\bar{C}_\gamma(\tau)$ with the same effective time delay, but the amplitude is reduced to the fraction $\left[1+4\pi^2\Delta_{\mathrm{tQ}}^{-1}(\tau)\xi^2\right]^{-1/2}$. This observation suggests the following correction of $\bar{C}_\gamma(\tau)$ when the molecular concentrations oscillate with a constant period T:

$$\bar{C}_{\gamma_{\mathrm{p}}}(\tau) \equiv \min\left\{\frac{\bar{C}_{\mathrm{tQ}}\left[\tau-\Delta_{\mathrm{tQ}}^{-1/2}(\tau)\right]-\langle\bar{C}_{\mathrm{tQ}}(\tau)\rangle}{\sqrt{1+4\left(\frac{\pi}{k_\delta T}\right)^2\Delta_{\mathrm{tQ}}^{-1}(\tau)}} + \langle\bar{C}_{\mathrm{tQ}}(\tau)\rangle, \bar{A}(\tau), \bar{B}(\tau)\right\}, \quad (27)$$

where $\langle\bar{C}_{\mathrm{tQ}}(\tau)\rangle$ is the time average of $\bar{C}_{\mathrm{tQ}}(\tau)$ over its period. As will be demonstrated later, $\bar{C}_{\gamma_{\mathrm{p}}}(\tau)$ in Eq. (27) offers a more correct description of periodic oscillations than $\bar{C}_\gamma(\tau)$, but we will focus on the use of $\bar{C}_\gamma(\tau)$ owing to its simpler form with wider applicability beyond periodic oscillations. Still, back to Eq. (26), this approach holds the potential for systematic improvements in the modeling accuracy.

B. Transcription factor–DNA binding case

Thus far, we have implicitly assumed the continuous nature of molecular concentrations as in Eq. (1) with the time derivative of $C(t)$. However, there exist biomolecular events that

fundamentally deviate from this assumption. For example, a transcription factor (TF) binds to a DNA molecule in the nucleus to regulate mRNA expression and the number of such a TF–DNA assembly would be either 1 or 0 for a particular DNA site, which can afford at most one copy of the TF. This inherently discrete nature of the TF–DNA binding number is seemingly contrasted with the continuity of the molecular complex level in Eq. (1). To rigorously describe this TF–DNA binding dynamics, we harness the chemical master equation [29] instead of Eq. (1).

In this formulation, $P(n,t)$ denotes the probability that n copies of the TF are occupying the target DNA site at time t. If this DNA site can afford at most N copies of the TF at once, $n = 0, 1, \cdots, N$ and $\sum_{n=0}^{N} P(n,t) = 1$. If we further define $P(n,t) \equiv 0$ for $n \neq 0, 1, \cdots, N$ and assume that the DNA-binding TFs are hardly accessible by molecular machineries such as for protein degradation, the temporal change of $P(n,t)$ with $n = 0, 1, \cdots, N$ is governed by this master equation:

$$\frac{\partial P(n,t)}{\partial t} = k_{\mathrm{a}} V \left[A_{\mathrm{TF}}(t) - \frac{n-1}{V}\right]\left(B_{\mathrm{DNA}} - \frac{n-1}{V}\right) P(n-1,t) - \left\{k_{\mathrm{a}} V \left[A_{\mathrm{TF}}(t) - \frac{n}{V}\right]\left(B_{\mathrm{DNA}} - \frac{n}{V}\right) + n k_{\delta}\right\} P(n,t) + (n+1) k_{\delta} P(n+1,t), \quad (28)$$

where k_{a} and k_{δ} denote the TF–DNA binding and unbinding rates, respectively [analogous to the parameters in Eq. (1)], V is the nuclear volume, $A_{\mathrm{TF}}(t)$ is the total TF concentration in the nucleus, and B_{DNA} is the "concentration" of the target DNA site, i.e., $B_{\mathrm{DNA}} = NV^{-1}$. Here, we assume $A_{\mathrm{TF}}(t) \gg B_{\mathrm{DNA}}$ for little stochasticity in $A_{\mathrm{TF}}(t)$ (i.e., $A_{\mathrm{TF}}(t)$ to be uniquely determined at each time t) and the cell growth is negligible for a steady nuclear volume (i.e., V to remain constant over time).

Introducing a quantity $C_{\mathrm{TF}}(t) \equiv \langle nV^{-1} \rangle = V^{-1} \sum_{n=0}^{N} n P(n,t)$ to Eq. (28) results in

$$\frac{\mathrm{d}C_{\mathrm{TF}}(t)}{\mathrm{d}t} = k_{\mathrm{a}} \sum_{n=0}^{N} \left[A_{\mathrm{TF}}(t) - \frac{n}{V}\right]\left(B_{\mathrm{DNA}} - \frac{n}{V}\right) P(n,t) - k_{\delta} C_{\mathrm{TF}}(t)$$
$$= k_{\mathrm{a}} \left\{[A_{\mathrm{TF}}(t) - C_{\mathrm{TF}}(t)][B_{\mathrm{DNA}} - C_{\mathrm{TF}}(t)] + \left\langle \left(\frac{n}{V}\right)^2 \right\rangle - \left\langle \frac{n}{V} \right\rangle^2 \right\} - k_{\delta} C_{\mathrm{TF}}(t), \quad (29)$$

where $\langle (nV^{-1})^2 \rangle = V^{-2} \sum_{n=0}^{N} n^2 P(n,t)$. Eq. (29) is reminiscent of Eq. (1), when the stochastic fluctuation in the TF binding $[\langle (nV^{-1})^2 \rangle - \langle nV^{-1} \rangle^2]$ is negligible. The stochastic fluctuation, however, cannot be ignored for small N. For simplicity, we will henceforth consider the case of $N = 1$ and thus of $B_{\mathrm{DNA}} = V^{-1}$. In this case, Eq. (29) is rewritten as

$$\frac{\mathrm{d}\bar{C}_{\mathrm{TF}}(\tau)}{\mathrm{d}\tau} = \frac{\bar{A}_{\mathrm{TF}}(\tau)}{KV} - [1 + \bar{A}_{\mathrm{TF}}(\tau)]\bar{C}_{\mathrm{TF}}(\tau) = [1 + \bar{A}_{\mathrm{TF}}(\tau)]\left[\bar{C}_{\mathrm{TFQ}}(\tau) - \bar{C}_{\mathrm{TF}}(\tau)\right], \quad (30)$$

where $\tau \equiv k_{\delta} t$ and $K \equiv k_{\delta}/k_{\mathrm{a}}$ as adopted in Eq. (2), $\bar{A}_{\mathrm{TF}}(\tau) \equiv A_{\mathrm{TF}}(t)/K$, $\bar{C}_{\mathrm{TF}}(\tau) \equiv C_{\mathrm{TF}}(t)/K$, and $\bar{C}_{\mathrm{TFQ}}(\tau)$ is given by

$$\bar{C}_{\mathrm{TFQ}}(\tau) \equiv \frac{\bar{A}_{\mathrm{TF}}(\tau)}{KV[1 + \bar{A}_{\mathrm{TF}}(\tau)]}. \quad (31)$$

In a similar fashion to the tQSSA in Sec. II.A, one may consider an estimate $\bar{C}_{\mathrm{TF}}(\tau) \approx \bar{C}_{\mathrm{TFQ}}(\tau)$, or equivalently, $C_{\mathrm{TF}}(t) \approx C_{\mathrm{TFQ}}(t)$ with this form:

$$C_{\mathrm{TFQ}}(t) \equiv \frac{A_{\mathrm{TF}}(t)}{V[K + A_{\mathrm{TF}}(t)]}. \quad (32)$$

$C_{\mathrm{TFQ}}(t)$ looks very similar to the MM rate law, regarding $B_{\mathrm{DNA}} = V^{-1}$. Nevertheless, $C_{\mathrm{TFQ}}(t)$ is not a mere continuum of Eq. (9), because the denominator in $C_{\mathrm{TFQ}}(t)$ includes $K + A_{\mathrm{TF}}(t)$, but not $K + A_{\mathrm{TF}}(t) + V^{-1}$ from $B_{\mathrm{DNA}} = V^{-1}$. In fact, the discrepancy between $C_{\mathrm{TFQ}}(t)$ and Eq. (9) comes from the inherent stochasticity in the TF–DNA binding dynamics in Eqs. (28) and (29). In this regard, directly relevant to $C_{\mathrm{TFQ}}(t)$ is the stochastic version of the MM rate law with denominator $K + A(t) + B(t) - V^{-1}$ proposed by Levine and Hwa [30]. $C_{\mathrm{TFQ}}(t)$ is a fundamentally more correct approximant for the DNA-binding TF level with $N = 1$ than both $C_{\mathrm{tQ}}(t)$ [Eq. (7)] and its descendant [Eq. (9)].

Still, the use of $C_{\mathrm{TFQ}}(t)$ to estimate $C_{\mathrm{TF}}(t)$ in Eq. (30) stands on the assumption that $C_{\mathrm{TF}}(t)$ approaches the equilibrium fast enough each time before the marked temporal change of $A_{\mathrm{TF}}(t)$. Following a similar procedure to Sec. II.A, we relieve this quasi-steady state

assumption and improve the approximation of $C_{\mathrm{TF}}(t)$ in the case of time-varying $A_{\mathrm{TF}}(t)$. Notice that the exact solution of Eq. (30) is

$$\bar{C}_{\mathrm{TF}}(\tau) = \int_{\tau_0}^{\tau} [1 + \bar{A}_{\mathrm{TF}}(\tau')]\bar{C}_{\mathrm{TFQ}}(\tau') e^{-\int_{\tau'}^{\tau}[1+\bar{A}_{\mathrm{TF}}(\tau'')]\mathrm{d}\tau''} \mathrm{d}\tau' + \bar{C}_{\mathrm{TF}}(\tau_0) e^{-\int_{\tau_0}^{\tau}[1+\bar{A}_{\mathrm{TF}}(\tau')]\mathrm{d}\tau'}, \quad (33)$$

where τ_0 denotes an arbitrarily assigned, initial point of τ. Assume that $1 + \bar{A}_{\mathrm{TF}}(\tau')$ changes rather slowly over τ' to satisfy

$$1 + \bar{A}_{\mathrm{TF}}(\tau') \approx 1 + \bar{A}_{\mathrm{TF}}(\tau) \text{ for } \tau' \text{ in the range } \tau - \frac{1}{1+\bar{A}_{\mathrm{TF}}(\tau)} \lesssim \tau' \leq \tau. \quad (34)$$

As we will show later, Eq. (34) is readily satisfied in physiologically-relevant conditions. With Eq. (34), Eq. (33) for $\tau \gg \tau_0 + [1 + \bar{A}_{\mathrm{TF}}(\tau_0)]^{-1}$ is approximated as

$$\bar{C}_{\mathrm{TF}}(\tau) \approx [1 + \bar{A}_{\mathrm{TF}}(\tau)] \int_{-\infty}^{\tau} \bar{C}_{\mathrm{TFQ}}(\tau') e^{-[1+\bar{A}_{\mathrm{TF}}(\tau)](\tau-\tau')} \mathrm{d}\tau'. \quad (35)$$

The Taylor expansion $\bar{C}_{\mathrm{TFQ}}(\tau') = \bar{C}_{\mathrm{TFQ}}(\tau) - (\tau - \tau')\bar{C}'_{\mathrm{TFQ}}(\tau) + (\tau - \tau')^2 \bar{C}''_{\mathrm{TFQ}}(\tau)/2 - \cdots$ leads Eq. (35) to

$$\begin{aligned}\bar{C}_{\mathrm{TF}}(\tau) &\approx \bar{C}_{\mathrm{TFQ}}(\tau) - \frac{1}{1 + \bar{A}_{\mathrm{TF}}(\tau)} \frac{\mathrm{d}\bar{C}_{\mathrm{TFQ}}(\tau)}{\mathrm{d}\tau} \int_0^{\infty} x e^{-x} \mathrm{d}x \\ &\quad + \frac{1}{2[1 + \bar{A}_{\mathrm{TF}}(\tau)]^2} \frac{\mathrm{d}^2\bar{C}_{\mathrm{TFQ}}(\tau)}{\mathrm{d}\tau^2} \int_0^{\infty} x^2 e^{-x} \mathrm{d}x - \cdots \\ &= \bar{C}_{\mathrm{TFQ}}(\tau) - \frac{1}{1+\bar{A}_{\mathrm{TF}}(\tau)} \frac{\mathrm{d}\bar{C}_{\mathrm{TFQ}}(\tau)}{\mathrm{d}\tau} + \frac{1}{[1+\bar{A}_{\mathrm{TF}}(\tau)]^2} \frac{\mathrm{d}^2\bar{C}_{\mathrm{TFQ}}(\tau)}{\mathrm{d}\tau^2} - \cdots \\ &= \bar{C}_{\mathrm{TFQe}}(\tau) + \frac{1}{[1+\bar{A}_{\mathrm{TF}}(\tau)]^2} \frac{\mathrm{d}^2\bar{C}_{\mathrm{TFQ}}(\tau)}{\mathrm{d}\tau^2} - \cdots, \end{aligned} \quad (36)$$

where $\bar{C}_{\mathrm{TFQe}}(\tau)$ is defined as

$$\bar{C}_{\mathrm{TFQe}}(\tau) \equiv \bar{C}_{\mathrm{TFQ}}(\tau) - \frac{1}{1+\bar{A}_{\mathrm{TF}}(\tau)} \frac{\mathrm{d}\bar{C}_{\mathrm{TFQ}}(\tau)}{\mathrm{d}\tau}. \quad (37)$$

In a similar way to Sec. II.A, we take the Taylor expansion of the time-delayed form of $\bar{C}_{\mathrm{TFQ}}(\tau)$:

$$\bar{C}_{\mathrm{TFQ}}\left[\tau - \frac{1}{1+\bar{A}_{\mathrm{TF}}(\tau)}\right] = \bar{C}_{\mathrm{TFQ}}(\tau) - \frac{1}{1+\bar{A}_{\mathrm{TF}}(\tau)} \frac{\mathrm{d}\bar{C}_{\mathrm{TFQ}}(\tau)}{\mathrm{d}\tau} + \frac{1}{2[1+\bar{A}_{\mathrm{TF}}(\tau)]^2} \frac{\mathrm{d}^2\bar{C}_{\mathrm{TFQ}}(\tau)}{\mathrm{d}\tau^2} - \cdots. \quad (38)$$

Interestingly, the zeroth-order and first-order derivative terms of $\bar{C}_{\mathrm{TFQ}}(\tau)$ on the right-hand side above are identical to $\bar{C}_{\mathrm{TFQe}}(\tau)$, and the second-order derivative term still covers a half of that term in Eq. (36). Hence, we propose the following approximant for $\bar{C}_{\mathrm{TF}}(\tau)$:

$$\bar{C}_{\mathrm{TF}\gamma}(\tau) \equiv \bar{C}_{\mathrm{TFQ}}\left[\tau - \frac{1}{1+\bar{A}_{\mathrm{TF}}(\tau)}\right]. \quad (39)$$

The corresponding approximant for $C_{\mathrm{TF}}(t)$ is

$$C_{\mathrm{TF}\gamma}(t) \equiv C_{\mathrm{TFQ}}\left[t - \frac{k_\delta^{-1}K}{K+A_{\mathrm{TF}}(t)}\right]. \quad (40)$$

As will be shown later, the accuracy of the approximant $\bar{C}_{\mathrm{TF}\gamma}(\tau)$ or $C_{\mathrm{TF}\gamma}(t)$ surpasses that of $\bar{C}_{\mathrm{TFQ}}(\tau)$ or $C_{\mathrm{TFQ}}(t)$. On the other hand, Eqs. (39) and (40) are ill-defined for $\tau - [1 + \bar{A}_{\mathrm{TF}}(\tau)]^{-1} < \tau_0$ where τ_0 is an initial point of τ. In fact, from the last term in Eq. (33), τ should satisfy $\tau \gg \tau_0 + [1 + \bar{A}_{\mathrm{TF}}(\tau_0)]^{-1}$ for the application of any rate law [e.g., Eq. (39), (40), or (32)] whose form does not depend on the initial conditions.

To clarify the preconditions for the use of $\bar{C}_{\mathrm{TF}\gamma}(\tau)$ or $C_{\mathrm{TF}\gamma}(t)$, we first revisit the condition in Eq. (34). Applying $1 + \bar{A}_{\mathrm{TF}}(\tau') \approx 1 + \bar{A}_{\mathrm{TF}}(\tau) + (\tau' - \tau)\bar{A}'_{\mathrm{TF}}(\tau)$ to Eq. (34) gives rise to this condition:

$$\varepsilon_{\mathrm{TF}}(\tau) \equiv \frac{\bar{A}_{\mathrm{TF}}(\tau)}{[1+\bar{A}_{\mathrm{TF}}(\tau)]^2} |\mu_{\mathrm{TF}}(\tau)| \ll 1, \quad (41)$$

where $\mu_{\mathrm{TF}}(\tau) \equiv \bar{A}'_{\mathrm{TF}}(\tau)/\bar{A}_{\mathrm{TF}}(\tau)$. Next, the comparison between Eqs. (36) and (38) shows the difference of $\sim\bar{C}''_{\mathrm{TFQ}}(\tau)/\{2[1 + \bar{A}_{\mathrm{TF}}(\tau)]^2\}$ and thereby offers this condition:

$$\varepsilon_{\mathrm{TF}\gamma}(\tau) \equiv \frac{1}{2[1+\bar{A}_{\mathrm{TF}}(\tau)]^2 \bar{C}_{\mathrm{TFQ}}\{\tau - [1+\bar{A}_{\mathrm{TF}}(\tau)]^{-1}\}} \left|\frac{\mathrm{d}^2\bar{C}_{\mathrm{TFQ}}(\tau)}{\mathrm{d}\tau^2}\right| \ll 1, \quad (42)$$

where $\bar{C}''_{\mathrm{TFQ}}(\tau)$ is obtained from Eq. (31) as

$$\frac{\mathrm{d}^2\bar{C}_{\mathrm{TFQ}}(\tau)}{\mathrm{d}\tau^2} = \frac{\bar{C}_{\mathrm{TFQ}}(\tau)}{1+\bar{A}_{\mathrm{TF}}(\tau)} \left[\frac{1-\bar{A}_{\mathrm{TF}}(\tau)}{1+\bar{A}_{\mathrm{TF}}(\tau)} \mu_{\mathrm{TF}}^2(\tau) + \frac{\mathrm{d}\mu_{\mathrm{TF}}(\tau)}{\mathrm{d}\tau}\right]. \quad (43)$$

In summary, our approximant $\bar{C}_{\mathrm{TF}\gamma}(\tau)$ shall work when Eqs. (41) and (42) are satisfied. As we will show later, Eq. (41) is in fact easy to satisfy and thus only Eq. (42) tends to serve as a key factor for the validity of $\bar{C}_{\mathrm{TF}\gamma}(\tau)$.

On the other hand, the MM-like formula $\bar{C}_{\mathrm{TFQ}}(\tau)$ would be valid in the following condition from Eq. (36), instead of the condition in Eq. (42):

$$\varepsilon_{\mathrm{TFQ}}(\tau) \equiv \frac{1}{\bar{C}_{\mathrm{TFQ}}(\tau)}\left|\frac{1}{1+\bar{A}_{\mathrm{TF}}(\tau)}\frac{\mathrm{d}\bar{C}_{\mathrm{TFQ}}(\tau)}{\mathrm{d}\tau} - \frac{1}{[1+\bar{A}_{\mathrm{TF}}(\tau)]^2}\frac{\mathrm{d}^2\bar{C}_{\mathrm{TFQ}}(\tau)}{\mathrm{d}\tau^2}\right| \ll 1, \quad (44)$$

where $\bar{C}'_{\mathrm{TFQ}}(\tau) = \mu_{\mathrm{TF}}(\tau)\bar{C}_{\mathrm{TFQ}}(\tau)/[1+\bar{A}_{\mathrm{TF}}(\tau)]$ from Eq. (31) and $\bar{C}''_{\mathrm{TFQ}}(\tau)$ is given by Eq. (43).

Following a similar procedure to Sec. II.A, we can further improve our TF–DNA binding description in a certain scenario. We apply the inverse Fourier transform $\bar{C}_{\mathrm{TFQ}}(\tau) = \int_{-\infty}^{\infty}\bar{C}^{\mathrm{f}}_{\mathrm{TFQ}}(\xi)e^{2\pi i\tau\xi}\mathrm{d}\xi$ to Eq. (35) and then obtain

$$\begin{aligned}\bar{C}_{\mathrm{TF}}(\tau) &\approx [1+\bar{A}_{\mathrm{TF}}(\tau)]e^{-[1+\bar{A}_{\mathrm{TF}}(\tau)]\tau}\int_{-\infty}^{\infty}\int_{-\infty}^{\tau}\bar{C}^{\mathrm{f}}_{\mathrm{TFQ}}(\xi)e^{[2\pi i\xi+1+\bar{A}_{\mathrm{TF}}(\tau)]\tau'}\mathrm{d}\tau'\mathrm{d}\xi \\ &= \int_{-\infty}^{\infty}\frac{\bar{C}^{\mathrm{f}}_{\mathrm{TFQ}}(\xi)}{\sqrt{1+4\pi^2[1+\bar{A}_{\mathrm{TF}}(\tau)]^{-2}\xi^2}}e^{i\left\{2\pi\tau\xi-\arctan\left\{2\pi\xi[1+\bar{A}_{\mathrm{TF}}(\tau)]^{-1}\right\}\right\}}\mathrm{d}\xi \\ &\approx \int_{-\infty}^{\infty}\frac{\bar{C}^{\mathrm{f}}_{\mathrm{TFQ}}(\xi)}{\sqrt{1+4\pi^2[1+\bar{A}_{\mathrm{TF}}(\tau)]^{-2}\xi^2}}e^{2\pi i\xi\{\tau-[1+\bar{A}_{\mathrm{TF}}(\tau)]^{-1}\}}\mathrm{d}\xi, \quad (45)\end{aligned}$$

where the last step takes $\arctan(x) \approx x$ for $|x| \ll 1$. Because $\bar{C}^{\mathrm{f}}_{\mathrm{TFQ}}(\xi)$ is the Fourier transform of $\bar{C}_{\mathrm{TFQ}}(\tau)$, the above result resembles $\bar{C}_{\mathrm{TF}\gamma}(\tau)$ with the same effective time delay, but the amplitude is reduced to the fraction $\{1+4\pi^2[1+\bar{A}_{\mathrm{TF}}(\tau)]^{-2}\xi^2\}^{-1/2}$. This observation suggests the following correction of $\bar{C}_{\mathrm{TF}\gamma}(\tau)$ when the TF level oscillates with a constant period T:

$$\bar{C}_{\mathrm{TF}\gamma_{\mathrm{p}}}(\tau) \equiv \frac{\bar{C}_{\mathrm{TFQ}}\{\tau-[1+\bar{A}_{\mathrm{TF}}(\tau)]^{-1}\}-\langle\bar{C}_{\mathrm{TFQ}}(\tau)\rangle}{\sqrt{1+4\left(\frac{\pi}{k_\delta T}\right)^2[1+\bar{A}_{\mathrm{TF}}(\tau)]^{-2}}} + \langle\bar{C}_{\mathrm{TFQ}}(\tau)\rangle, \quad (46)$$

where $\langle\bar{C}_{\mathrm{TFQ}}(\tau)\rangle$ is the time average of $\bar{C}_{\mathrm{TFQ}}(\tau)$ over its period. We will later demonstrate that $\bar{C}_{\mathrm{TF}\gamma_{\mathrm{p}}}(\tau)$ in Eq. (46) is more accurate for periodic oscillations than $\bar{C}_{\mathrm{TF}\gamma}(\tau)$, but will mainly use $\bar{C}_{\mathrm{TF}\gamma}(\tau)$ owing to its simpler form with wider applicability beyond periodic oscillations.

III. BIOPHYSICAL APPLICATIONS

In Sec. II, we derived the revised versions of the MM rate law for time-varying concentrations of molecular components. Here, we will apply this revised rate law to a number of biomolecular processes, in comparison with the existing approaches—the tQSSA and sQSSA. In Secs. III.A–III.D, we will focus on the approximation of quantitative dynamical profiles, and in Secs. III.E and III.F on the prediction for qualitatively new dynamical patterns not expected by the existing approaches.

A. Biochemical reaction and transport

Imagine that substrate A binds to enzyme B, which catalyzes a metabolic reaction to convert A to another molecule. The formation of the enzyme–substrate complex follows Eq. (1) or its equivalent Eq. (2). In Eq. (1), we set $k_\delta = k_{\mathrm{d}} + r_{\mathrm{c}}$ where r_{c} is interpreted as the catalytic rate constant of the reaction (conventionally written as k_{cat} in literature), and $k_{\mathrm{loc}} = k_{\mathrm{dlt}} = 0$. In this system, the total substrate concentration $A(t)$ changes over time as

$$\frac{\mathrm{d}A(t)}{\mathrm{d}t} = -r_{\mathrm{c}}C(t), \quad (47)$$

which is equivalent to

$$\mu_{\mathrm{A}}(\tau) = -\frac{r_{\mathrm{c}}}{k_\delta}\frac{\bar{C}(\tau)}{\bar{A}(\tau)}. \quad (48)$$

$\mu_{\mathrm{A}}(\tau)$ is defined in Sec. II.A as $\mu_{\mathrm{A}}(\tau) \equiv \bar{A}'(\tau)/\bar{A}(\tau)$. We further assume that the total enzyme concentration is constant over time [$\bar{B}(\tau) = \bar{B}$ and $\mu_{\mathrm{B}}(\tau) = 0$ when $\mu_{\mathrm{B}}(\tau) \equiv \bar{B}'(\tau)/\bar{B}(\tau)$ as defined in Sec. II.A]. Eqs. (2) and (48) fully determine the time course of the system with given initial conditions and parameters.

Unlike other molecular events that we will consider later, the majority of known metabolic reactions are likely to be modeled by the sQSSA or tQSSA to a sufficient degree, without the need for our proposed formula $C_\gamma(t)$ in Eq. (19) [or equivalently, $\bar{C}_\gamma(\tau)$ in Eq. (18)]. Indeed, (*i*) most enzymatic reactions in Table S1 satisfy Eq. (25) as well as Eqs. (20) and (22) (i.e., $\varepsilon_1, \varepsilon_2, \varepsilon_{\mathrm{tQ}} \ll 1$ in Table S1), although a malate dehydrogenase does not follow Eq. (25) very well when the substrate is oxaloacetate, and (*ii*) the enzyme levels in Table S1 are generally much lower than the substrate levels, despite two exceptions of malate dehydrogenase and succinate dehydrogenase (fumarate as a substrate). According to the discussion in Sec. II.A, these (*i*) and (*ii*) indicate that the tQSSA [relevant to (*i*)] or sQSSA [relevant to (*i*) and (*ii*)] would often suffice for the kinetic modeling of metabolic reactions. Of note, the sQSSA has long been considered as suitable for the modeling of metabolic reactions [1–3]. Yet, as we will analyze below, the malate dehydrogenase kinetics is precisely described by our formula $C_\gamma(t)$, whereas the tQSSA and sQSSA perform rather erroneously.

In addition, we examine the case of nutrient transport into a cell, where an "enzyme" is a transporter protein on the cell surface and a substrate is a small molecule nutrient in the extracellular environment. r_{c} is then interpreted as the uptake rate of a transporter-binding nutrient. We assume that as the cells reproduce, the transporters increase over time with constant $\mu_{\mathrm{B}}(\tau) = \mu_{\mathrm{B}}$, which is equal to the cell growth rate divided by k_δ. With this $\mu_{\mathrm{B}}(\tau)$, Eqs. (2) and (48) govern the full kinetics of the nutrient transport. Our analysis of the well-documented, phosphotransferase system (PTS) in bacterium *Escherichia coli* reveals that the sQSSA alone would suffice to describe this system without the need for $C_\gamma(t)$, as in Table S2 where $\varepsilon_1, \varepsilon_2, \varepsilon_{\mathrm{tQ}} \ll 1$ and the transporter level is far below the nutrient level.

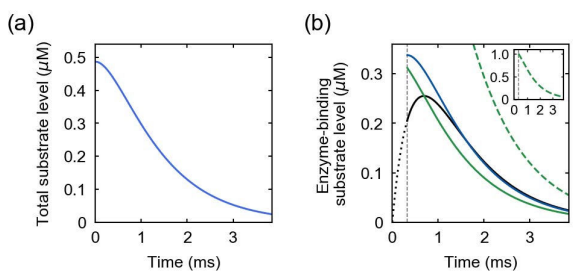

FIG. 1. Oxaloacetate (substrate) conversion by malate dehydrogenase (enzyme). (a) The total substrate concentration over time, calculated by Eqs. (2) and (48) (Text S2). The initial substrate concentration is set as the substrate concentration in Table S1. (b) The enzyme-binding substrate concentrations calculated by Eq. (2) (black solid line; black dotted line for a transient period described below), by our revised MM rate law (blue solid line), by the tQSSA (green solid line), and by the sQSSA (green dashed line) (Text S2). These calculations are based on the total substrate concentration in (a). An inset shows a more complete range of the enzyme-binding substrate concentration from the sQSSA. In (a) and (b), we used the parameters and total enzyme concentration in Table S1. When solving Eqs. (2) and (48), the initial concentration of the enzyme-binding substrate was set to zero. As discussed in Sec. II.A, any form of a rate law without the initial-condition dependency would only work for $t \gg k_\delta^{-1}\Delta_{\mathrm{tQ}}^{-1/2}(0)$, and also our revised MM rate law is ill-defined for a period $t < k_\delta^{-1}\Delta_{\mathrm{tQ}}^{-1/2}(t)$; therefore, for the right comparison with our revised rate law, (b) presents the tQSSA and sQSSA results only after $t = k_\delta^{-1}\Delta_{\mathrm{tQ}}^{-1/2}(t)$ (vertical dashed line).

As mentioned above, Table S1 indicates that oxaloacetate conversion by malate dehydrogenase would be well described by our revised MM rate law [$C_\gamma(t)$], compared to the tQSSA and sQSSA. Indeed, the time trajectory of $C_\gamma(t)$ shows remarkable agreement with the simulated enzyme-binding substrate levels [$C(t)$] from Eqs. (2) and (48), after some transient period of $C(t)$ that depends on the initial condition (Fig. 1 and Text S2); meanwhile, the tQSSA is ~0.3-ms more advanced than $C(t)$ in the overall profile and the sQSSA severely overestimates $C(t)$ [Fig. 1(b)]. For example, at $t = 1.9$ ms, $C(t) \approx C_\gamma(t) = 0.13$ μM and the sQSSA leads to 0.31 μM, while the tQSSA results in 0.13 μM at $t = 1.6$ ms [Fig. 1(b)]. The overall time shift of the tQSSA from $C(t)$ is caused by the discarding of the time delay [$\sim k_\delta^{-1}\Delta_{\mathrm{tQ}}^{-1/2}(t)$] in enzyme–substrate complex formation in the tQSSA, and the overestimation of $C(t)$ by the sQSSA comes from the unlimited enzyme–substrate binding with the increasing enzymes $\{A(t)B(t)/[K + A(t)]\}$ in the sQSSA.

To conclude, our revised MM rate law provides quantitatively better approximation of the above malate dehydrogenase kinetics than the existing approaches, although the latter are likely to be sufficient for the modeling of many metabolic reaction and transport systems. In the case of protein–protein and TF–DNA interactions, the utility of the revised rate law is more prominent, as we will address below.

B. Protein–protein interaction

Next, we move to the case of protein–protein interactions. The interacting proteins often show the concentrations comparable with each other [15–17], and thus the tQSSA, not the sQSSA, has recently been recommended for the modeling of their interactions [12,18]. Here, we will focus on the interactions between proteins whose abundances oscillate over time with circadian rhythmicity, i.e., ~24-h periodicity. Circadian protein oscillations play a pivotal role in coordinating numerous physiological processes [25,26]. Such time-varying nature in protein abundances might even challenge the relevance of the tQSSA and would serve as a testbed for our revised MM rate law $\bar{C}_\gamma(\tau)$ in Eq. (18).

Suppose that proteins A and B have oscillating concentrations with sinusoidal forms:

$$\overline{A}(\tau) = \overline{A}_{\max}\left\{1 - \frac{\alpha_{\mathrm{A}}}{2}\left[1 + \cos\left(\frac{2\pi}{k_\delta T}\tau\right)\right]\right\} \text{ and } \overline{B}(\tau) = \overline{B}_{\max}\left\{1 - \frac{\alpha_{\mathrm{B}}}{2}\left[1 + \cos\left(\frac{2\pi}{k_\delta T}\tau - \varphi_{\mathrm{B}}\right)\right]\right\}, \tag{49}$$

where $\overline{A}_{\max}$ ($\overline{B}_{\max}$), $\alpha_{\mathrm{A(B)}}$, T, and φ_{B} denote the peak level of $\overline{A}(\tau)$ [$\overline{B}(\tau)$], the peak-to-trough difference of $\overline{A}(\tau)$ [$\overline{B}(\tau)$] divided by the peak level, the oscillation period of a circadian or diurnal rhythm, and the phase difference between $\overline{A}(\tau)$ and $\overline{B}(\tau)$, respectively. Here, α_{A} and α_{B} range from 0 to 1 (the closer they are to 1, the stronger the oscillations) and $0 \le \varphi_{\mathrm{B}} \le \pi$ without loss of generality. Throughout this study, we choose $T = 24$ h. Based on $\overline{A}(\tau)$ and $\overline{B}(\tau)$ in Eq. (49), we numerically solve Eq. (2) to obtain $\bar{C}(\tau)$ (Text S2), and evaluate how well $\bar{C}(\tau)$ is approximated by each of $\bar{C}_\gamma(\tau)$, the tQSSA $\bar{C}_{\mathrm{tQ}}(\tau)$ in Eq. (5), and the sQSSA in Eq. (9). Regarding the periodic nature of this dynamics, we also examine the improved version of $\bar{C}_\gamma(\tau)$ for the periodic case, i.e., $\bar{C}_{\gamma_{\mathrm{p}}}(\tau)$ in Eq. (27).

As illustrated in Fig. 2(a), we observe that $\bar{C}_\gamma(\tau)$ and $\bar{C}_{\gamma_{\mathrm{p}}}(\tau)$ tend to better match the temporal trajectory of $\bar{C}(\tau)$ than the tQSSA and sQSSA. Additionally, $\bar{C}_{\gamma_{\mathrm{p}}}(\tau)$ in Fig. 2(a) exhibits a more correct amplitude than $\bar{C}_\gamma(\tau)$, as will be addressed later. For systematic evaluation, we define ϕ_γ^t, $\phi_{\gamma_{\mathrm{p}}}^t$, ϕ_{tQ}^t, and ϕ_{sQ}^t as the phase differences in hours between $\bar{C}_\gamma(\tau)$ and $\bar{C}(\tau)$, between $\bar{C}_{\gamma_{\mathrm{p}}}(\tau)$ and $\bar{C}(\tau)$, between the tQSSA and $\bar{C}(\tau)$, and between the sQSSA and $\bar{C}(\tau)$, respectively (Text S2). The sign of a given phase difference is assigned positive (negative) if the corresponding trajectory has a more advanced (delayed) phase than $\bar{C}(\tau)$. We observe that the signs of ϕ_{tQ}^t and ϕ_{sQ}^t are always positive and the signs of ϕ_γ^t and $\phi_{\gamma_{\mathrm{p}}}^t$ are

mostly negative. In the example of Fig. 2(a), $\phi_{\gamma}^{t} = -1.0$ h, $\phi_{\gamma_{\mathrm{p}}}^{t} = -0.95$ h, $\phi_{\mathrm{tQ}}^{t} = 3.05$ h, $\phi_{\mathrm{sQ}}^{t} = 3.1$ h, and hence $|\phi_{\gamma}^{t}|$ and $|\phi_{\gamma_{\mathrm{p}}}^{t}|$ are smaller than $|\phi_{\mathrm{tQ}}^{t}|$ and $|\phi_{\mathrm{sQ}}^{t}|$. We did find that $|\phi_{\gamma}^{t}|$ and $|\phi_{\gamma_{\mathrm{p}}}^{t}|$ tend to be smaller than $|\phi_{\mathrm{tQ}}^{t}|$ and $|\phi_{\mathrm{sQ}}^{t}|$ across physiologically-relevant conditions [Fig. 2(b) and $P < 10^{-4}$; see Table S3 and Text S2]. Because $\phi_{\gamma_{\mathrm{p}}}^{t}$ takes a value almost identical to ϕ_{γ}^{t} as expected from Eqs. (18) and (27), we will skip the further discussion of $\phi_{\gamma_{\mathrm{p}}}^{t}$. Remarkably, when $|\phi_{\gamma}^{t}|$, $|\phi_{\mathrm{tQ}}^{t}|$, or $|\phi_{\mathrm{sQ}}^{t}|$ is ≥1 h, most parameter conditions (86.2%) have $|\phi_{\gamma}^{t}|$ less than both $|\phi_{\mathrm{tQ}}^{t}|$ and $|\phi_{\mathrm{sQ}}^{t}|$ at least by one hour, and some of them (22.9%) even at least by two hours [Figs. 2(c) and 2(d); $P < 10^{-4}$ and Text S2]. These findings establish the tendency that $\bar{C}_{\gamma}(\tau)$, as well as $\bar{C}_{\gamma_{\mathrm{p}}}(\tau)$, is more likely to resemble $\bar{C}(\tau)$ in the phase than the tQSSA and sQSSA.

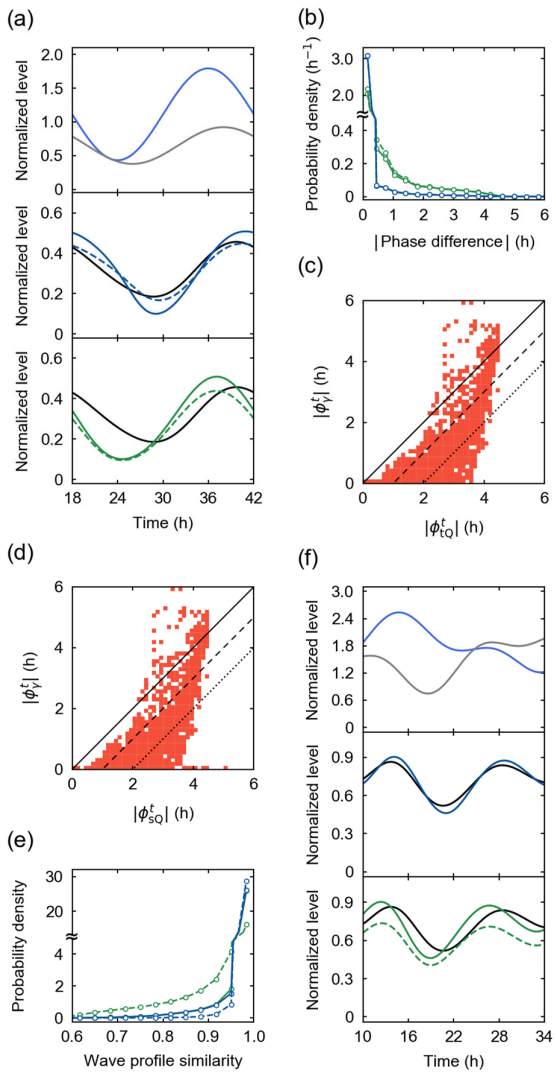

FIG. 2. Protein–protein interaction modeling. (a) Example time series of $\bar{A}(\tau)$ (bluish) and $\bar{B}(\tau)$ (gray) at the top, $\bar{C}(\tau)$ (black), $\bar{C}_{\gamma}(\tau)$ (blue solid line), and $\bar{C}_{\gamma_{\mathrm{p}}}(\tau)$ (blue dashed line) at the center, and $\bar{C}(\tau)$ (black), the tQSSA $\bar{C}_{\mathrm{tQ}}(\tau)$ (green solid line), and the sQSSA (green dashed line) at the bottom. The calculations are based on Eqs. (2), (5), (9), (18), (27), and (49), and $t = k_{\delta}^{-1}\tau$ as defined in Sec. II.A. (b) Probability distributions of $|\phi_{\gamma}^{t}|$ (blue solid line), $|\phi_{\gamma_{\mathrm{p}}}^{t}|$ (blue dashed line), $|\phi_{\mathrm{tQ}}^{t}|$ (green solid line), and

$|\phi_{\mathrm{sQ}}^t|$ (green dashed line) over randomly-sampled parameter sets in Table S3. Those of $|\phi_\gamma^t|$ and $|\phi_{\gamma_\mathrm{p}}^t|$ highly overlap and are not visually distinguishable here. (c,d) Scatter plot of $|\phi_{\mathrm{tQ}}^t|$ and $|\phi_\gamma^t|$ (c), or that of $|\phi_{\mathrm{sQ}}^t|$ and $|\phi_\gamma^t|$ (d), when $|\phi_\gamma^t|$, $|\phi_{\mathrm{tQ}}^t|$, or $|\phi_{\mathrm{sQ}}^t|$ is ≥1 h with randomly-sampled parameter sets in Table S3. A solid diagonal line corresponds to $|\phi_\gamma^t| = |\phi_{\mathrm{tQ}}^t|$ (c) or $|\phi_\gamma^t| = |\phi_{\mathrm{sQ}}^t|$ (d), a dashed diagonal line to $|\phi_\gamma^t| = |\phi_{\mathrm{tQ}}^t| - 1\mathrm{h}$ (c) or $|\phi_\gamma^t| = |\phi_{\mathrm{sQ}}^t| - 1\mathrm{h}$ (d), and a dotted diagonal line to $|\phi_\gamma^t| = |\phi_{\mathrm{tQ}}^t| - 2\mathrm{h}$ (c) or $|\phi_\gamma^t| = |\phi_{\mathrm{sQ}}^t| - 2\,\mathrm{h}$ (d). Although not covered in (b) and (d), $|\phi_{\mathrm{sQ}}^t| > 6\,\mathrm{h}$ for a tiny portion of the parameter sets (0.03%), in which still $|\phi_\gamma^t|, |\phi_{\mathrm{tQ}}^t| \leq 1\mathrm{h}$. (e) Probability distributions of S_γ (blue solid line), S_{γ_p} (blue dashed line), S_{tQ} (green solid line), and S_{sQ} (green dashed line) over randomly-sampled parameter sets in Table S3. (f) When based on Eq. (50), example time series of $\bar{A}(\tau)$ (bluish) and $\bar{B}(\tau)$ (gray) at the top, $\bar{C}(\tau)$ (black) and $\bar{C}_\gamma(\tau)$ (blue) at the center, and $\bar{C}(\tau)$ (black), the tQSSA $\bar{C}_{\mathrm{tQ}}(\tau)$ (green solid line), and the sQSSA (green dashed line) at the bottom. They were calculated in the same way as (a), except for the use of Eq. (50) instead of Eq. (49). For the detailed methods in (a)–(f) and the parameters in (a) and (f), refer to Text S2.

Other than phases, wave profiles (determined by the waveforms and peak levels) are the important features of oscillatory molecular behaviors. Therefore, we define similarity S_γ between the profiles of $\bar{C}_\gamma(\tau)$ and $\bar{C}(\tau)$ by aligning their phases to the same (Text S2). S_γ is devised to approach 1 away from 0, as the two wave profiles quantitatively better match each other. We also define the similarity measures S_{γ_p}, S_{tQ}, and S_{sQ} for $\bar{C}_{\gamma_\mathrm{p}}(\tau)$ and $\bar{C}(\tau)$, for the tQSSA and $\bar{C}(\tau)$, and for the sQSSA and $\bar{C}(\tau)$, respectively (Text S2). In the example of Fig. 2(a), $S_\gamma = 0.86$, $S_{\gamma_\mathrm{p}} = 0.97$, $S_{\mathrm{tQ}} = 0.86$, and $S_{\mathrm{sQ}} = 0.83$. Based on Eq. (18), one can expect that the main difference between $\bar{C}_\gamma(\tau)$ and $\bar{C}_{\mathrm{tQ}}(\tau)$ would be attributed to their phases, rather than to their shapes. As expected, S_γ and S_{tQ} tend to be almost equal to each other [Spearman's $\rho = 0.89$ and $P < 10^{-4}$; see Fig. 2(e) and Text S2]. Notably, S_{γ_p} exceeds S_γ and S_{tQ} in most cases (> 98%) because of the more correct amplitude of $\bar{C}_{\gamma_\mathrm{p}}(\tau)$ in Eq. (27). This result comes with relatively high S_{γ_p} values in Fig. 2(e) ($P < 10^{-4}$ and Text S2). On the other hand, consistent with the previous suggestions that the tQSSA is more accurate than the sQSSA [12], S_{sQ} tends to be below S_γ and S_{tQ} [Fig. 2(e); $P < 10^{-4}$ and Text S2]. Therefore, $\bar{C}_\gamma(\tau)$ and the tQSSA better approximate the wave profile of $\bar{C}(\tau)$ than the sQSSA.

To summarize, our revised rate law $\bar{C}_\gamma(\tau)$ tends to serve as a good approximant for $\bar{C}(\tau)$, with a more accurate phase than the tQSSA and sQSSA's and with a wave profile as accurate as the tQSSA's. $\bar{C}_\gamma(\tau)$ further improves to the form of $\bar{C}_{\gamma_\mathrm{p}}(\tau)$. One may expect that the high accuracy of $\bar{C}_\gamma(\tau)$ compared to the tQSSA's might be indicated by the range of its valid conditions in Eqs. (20), (22), and (23). In fact, most of the physiologically-relevant conditions in Table S3 (88.1%) satisfy both $\max_\tau[\varepsilon_1(\tau)] \leq 0.1$ and $\max_\tau[\varepsilon_2(\tau)] \leq 0.1$, and therefore only $\varepsilon_\gamma(\tau)$ and $\varepsilon_{\mathrm{tQ}}(\tau)$ remain the key determinants of the validities of $\bar{C}_\gamma(\tau)$ and the tQSSA, respectively. Our analysis reveals that $\max_\tau[\varepsilon_\gamma(\tau)] \leq 0.1$ for 55.9% of the simulated conditions and $\max_\tau[\varepsilon_{\mathrm{tQ}}(\tau)] \leq 0.1$ for 45.4% of the same conditions, supporting the wider applicability of $\bar{C}_\gamma(\tau)$ than the tQSSA's. Naturally, $\max_\tau[\varepsilon_\gamma(\tau)]$ and $\max_\tau[\varepsilon_{\mathrm{tQ}}(\tau)]$ correlate positively with $|\phi_\gamma^t|$ and $|\phi_{\mathrm{tQ}}^t|$, respectively (Spearman's $\rho = 0.52$ between $\max_\tau[\varepsilon_\gamma(\tau)]$ and $|\phi_\gamma^t|$ with $P < 10^{-4}$, and $\rho = 0.74$ between $\max_\tau[\varepsilon_{\mathrm{tQ}}(\tau)]$ and $|\phi_{\mathrm{tQ}}^t|$ with $P < 10^{-4}$; see Text S2).

Although physiologically less relevant, the oscillatory protein levels with irregular rhythmicity may provide another testbed for the approximating capability of $\bar{C}_\gamma(\tau)$. Hence, instead of Eq. (49), we consider the following $\overline{A}(\tau)$ and $\overline{B}(\tau)$ and numerically solve Eq. (2):

$$\overline{A}(\tau) = \frac{1}{N}\sum_{i=1}^{N} \overline{A}_{\max,i}\left\{1 - \frac{\alpha_{\mathrm{A},i}}{2}\left[1 + \cos\left(\frac{2\pi}{k_\delta T_{\mathrm{A},i}}\tau - \varphi_{\mathrm{A},i}\right)\right]\right\},$$
$$\overline{B}(\tau) = \frac{1}{N}\sum_{i=1}^{N} \overline{B}_{\max,i}\left\{1 - \frac{\alpha_{\mathrm{B},i}}{2}\left[1 + \cos\left(\frac{2\pi}{k_\delta T_{\mathrm{B},i}}\tau - \varphi_{\mathrm{B},i}\right)\right]\right\}. \quad (50)$$

We further choose $N = 10$ and randomly select the other parameters from the ranges in Text S2. Still, we find that $\bar{C}_\gamma(\tau)$ tends to better approximate even such an irregular profile of $\overline{C}(\tau)$ than the tQSSA and sQSSA, as illustrated in Fig. 2(f).

Next, we move to a real-world example of oscillating-protein interactions. In plant *Arabidopsis thaliana*, ZEITLUPE (ZTL) is an essential protein for a normal circadian periodicity. ZTL is stabilized by a direct interaction with another protein GIGANTEA (GI), and this interaction is enhanced by blue light [31–33]. As a result, ZTL protein levels oscillate in light–dark cycles, despite the constitutive mRNA expression of ZTL [31]. We here assess how well our revised MM rate law accounts for the experimental ZTL profile over time, through the modeling of the ZTL–GI interaction. If $A(t)$ and $B(t)$ represent the ZTL and GI concentrations, respectively, then the ZTL turnover dynamics can be described by the following equation:

$$\frac{\mathrm{d}A(t)}{\mathrm{d}t} = g_\mathrm{A} - r_\mathrm{c}C(t) - r_\mathrm{A}[A(t) - C(t)], \quad (51)$$

where g_A is the ZTL synthesis rate, $C(t)$ is the concentration of ZTL–GI complex, and r_A and r_c denote the degradation rates of free ZTL and GI-binding ZTL, respectively. $r_\mathrm{c} < r_\mathrm{A}$ because GI stabilizes ZTL. We assume $k_\delta = k_\mathrm{d} + r_\mathrm{c}$ and $C(t)$ is determined by Eq. (1). Because blue light enhances the ZTL–GI interaction, we assume that k_d and K in light do not exceed k_d and K in darkness, respectively. We set $B(t)$ as the known GI profile [Fig. 3(a)] [31] multiplied by a scaling coefficient w_GI, because the original GI profile is given by the concentration levels at a relative scale, not at the absolute scale. For the same reason, when comparing $A(t)$ with the experimental ZTL profile [Fig. 3(a)] [31], we use $A_\mathrm{s}(t) \equiv A(t)/w_\mathrm{ZTL}$ where w_ZTL is another scaling coefficient.

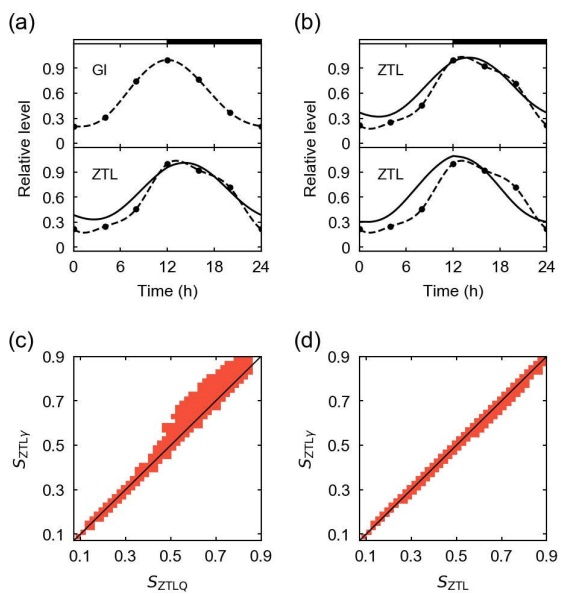

FIG. 3. ZTL–GI interaction in *Arabidopsis*. (a) The experimental GI levels (dots) [31] and their interpolation (dashed line) at the top, and the experimental ZTL levels (dots) [31], their interpolation (dashed line), and version (*i*)-based $A_\mathrm{s}(t)$ (solid line) at the bottom. (b) The experimental ZTL levels (dots) and their interpolation (dashed line) in (a), together with $A_\mathrm{s}(t)$ (solid line) from version (*ii*) at the top, or version (*iii*) at the bottom. In (a) and (b), $A_\mathrm{s}(t)$ and versions (*i*)–(*iii*) are defined in Sec. III.B and were computed with a given parameter set in Text S2. Horizontal white and black segments in (a) and (b) correspond to light and dark intervals, respectively. (c,d) Scatter plot of S_ZTLQ and $S_{\mathrm{ZTL}\gamma}$ (c), or that of S_ZTL and $S_{\mathrm{ZTL}\gamma}$ (d), over randomly-selected parameter sets in Table S4. A diagonal line corresponds to $S_{\mathrm{ZTL}\gamma} = S_\mathrm{ZTLQ}$ (c) or $S_{\mathrm{ZTL}\gamma} = S_\mathrm{ZTL}$ (d). For the detailed methods in (a)–(d), refer to Text S2.

We compute three different versions of $A(t)$ for their comparison with the experimental ZTL profile: (*i*) the first version is the solution of $A(t)$ from Eqs. (1) and (51), (*ii*) the second version is the solution of only Eq. (51) with the replacement of $C(t)$ by $C_\gamma(t)$ in Eq. (19), and (*iii*) the last version is similar to version (*ii*), but with the replacement of $C(t)$ by $C_{\mathrm{tQ}}(t)$ in Eq. (7). In other words, version (*i*) is the full modeling result that we treat as the gold standard to assess the relative accuracies of versions (*ii*) and (*iii*) from our revised MM rate law and the tQSSA, respectively. We do not longer consider the sQSSA because the tQSSA has already proven to be more accurate than the sQSSA in the previous studies [12,13,18–24] as well as in our analysis above (Sec. II.A. and Figs. 1 and 2).

We compute versions (*i*)–(*iii*) for randomly-selected parameters g_{A}, r_{A}, r_{c}, w_{GI}, and w_{ZTL} with k_{d} and K in light and darkness (Table S4 and Text S2). We define similarity S_{ZTL} between $A_{\mathrm{s}}(t)$ and the empirical ZTL profile when $A_{\mathrm{s}}(t)$ is calculated from version (*i*) by the above relation $A_{\mathrm{s}}(t) = A(t)/w_{\mathrm{ZTL}}$ (Text S2). S_{ZTL} is devised to approach 1 away from 0, as $A_{\mathrm{s}}(t)$ quantitatively better matches the ZTL profile. Analogously, $S_{\mathrm{ZTL}\gamma}$ and S_{ZTLQ} are defined for the cases with versions (*ii*) and (*iii*), respectively (Text S2). Figs. 3(a) and 3(b) present an example that $A_{\mathrm{s}}(t)$ from version (*ii*) is as close to the experimental ZTL profile as $A_{\mathrm{s}}(t)$ from version (*i*), and is closer to that experimental profile than $A_{\mathrm{s}}(t)$ from version (*iii*) ($S_{\mathrm{ZTL}} = 0.88$, $S_{\mathrm{ZTL}\gamma} = 0.88$, and $S_{\mathrm{ZTLQ}} = 0.79$). Indeed, most of our simulated conditions (78.2%) show $S_{\mathrm{ZTL}\gamma}$ higher than S_{ZTLQ} [Fig. 3(c); $P < 10^{-4}$ and Text S2], while $S_{\mathrm{ZTL}\gamma}$ and S_{ZTL} are almost the same as each other through the simulated conditions [Fig. 3(d)]. We hence conclude that our revised MM rate law is comparable with the full kinetic modeling in quantitative accounting for the experimental ZTL profile, with an improvement on the tQSSA.

C. TF–DNA interaction

We now examine the case of TF–DNA interactions. Suppose that the TF concentration oscillates over time in a sinusoidal form:

$$\overline{A}_{\mathrm{TF}}(\tau) = \overline{A}_{\mathrm{max}}\left\{1 - \frac{\alpha_{\mathrm{A}}}{2}\left[1 + \cos\left(\frac{2\pi}{k_\delta T}\tau\right)\right]\right\}, \quad (52)$$

where $\overline{A}_{\mathrm{max}}$, α_{A}, and T are defined the same as in Eq. (49). Based on $\overline{A}_{\mathrm{TF}}(\tau)$ in Eq. (52), we numerically solve Eq. (30) to obtain $\overline{C}_{\mathrm{TF}}(\tau)$ (Text S2), and evaluate how well $\overline{C}_{\mathrm{TF}}(\tau)$ is approximated by our formula $\bar{C}_{\mathrm{TF}\gamma}(\tau)$ in Eq. (39) or by the MM-like formula $\bar{C}_{\mathrm{TFQ}}(\tau)$ in Eq. (31). Regarding $\bar{C}_{\mathrm{TFQ}}(\tau)$, note that the distinction between the tQSSA and sQSSA is meaningless here because of condition $A_{\mathrm{TF}}(t) \gg B_{\mathrm{DNA}}$ in Sec. II.B. Given the periodic nature of the dynamics here, we also examine the improved version of $\bar{C}_{\mathrm{TF}\gamma}(\tau)$ for the periodic case, i.e., $\bar{C}_{\mathrm{TF}\gamma_{\mathrm{p}}}(\tau)$ in Eq. (46).

As illustrated in Fig. 4(a), we observe that $\bar{C}_{\mathrm{TF}\gamma}(\tau)$ and $\bar{C}_{\mathrm{TF}\gamma_{\mathrm{p}}}(\tau)$ tend to better match the time trajectory of $\bar{C}_{\mathrm{TF}}(\tau)$ than $\bar{C}_{\mathrm{TFQ}}(\tau)$. Additionally, $\bar{C}_{\mathrm{TF}\gamma_{\mathrm{p}}}(\tau)$ in Fig. 4(a) shows a very correct amplitude, as will be addressed later. In a similar fashion to Sec. III.B, we use quantities ϕ_γ^t, $\phi_{\gamma_{\mathrm{p}}}^t$, and ϕ_{Q}^t as the phase differences in hours between $\bar{C}_{\mathrm{TF}\gamma}(\tau)$ and $\overline{C}_{\mathrm{TF}}(\tau)$, between $\bar{C}_{\mathrm{TF}\gamma_{\mathrm{p}}}(\tau)$ and $\overline{C}_{\mathrm{TF}}(\tau)$, and between $\bar{C}_{\mathrm{TFQ}}(\tau)$ and $\overline{C}_{\mathrm{TF}}(\tau)$, respectively (Text S2). The magnitudes of these phase differences reach up to ~5 h in physiologically-relevant parameter conditions [Fig. 4(b) and Table S3]. The sign of a given phase difference is assigned positive (negative) if the corresponding trajectory has a more advanced (delayed) phase than $\bar{C}_{\mathrm{TF}}(\tau)$. In the simulated conditions (Table S3), we observe $\phi_{\mathrm{Q}}^t \geq 0$ and $\phi_\gamma^t, \phi_{\gamma_{\mathrm{p}}}^t \leq 0$. In the example of Fig. 4(a), $\phi_\gamma^t = \phi_{\gamma_{\mathrm{p}}}^t = -0.3$ h and $\phi_{\mathrm{Q}}^t = 2.3$ h, and here $|\phi_\gamma^t|$ and $|\phi_{\gamma_{\mathrm{p}}}^t|$ are smaller than $|\phi_{\mathrm{Q}}^t|$. Indeed, our analysis suggests that $|\phi_\gamma^t|$ and $|\phi_{\gamma_{\mathrm{p}}}^t|$ tend to be smaller than $|\phi_{\mathrm{Q}}^t|$ over the physiologically-relevant conditions [Fig. 4(b); $P < 10^{-4}$ and Text S2]. Because $\phi_{\gamma_{\mathrm{p}}}^t$ takes a value almost identical to ϕ_γ^t as expected from Eqs. (39) and (46), we will skip the further

discussion of $\phi_{\gamma_\mathrm{p}}^t$. When $|\phi_\gamma^t|$ or $|\phi_\mathrm{Q}^t|$ is ≥1 h, most parameter conditions (91.6%) have $|\phi_\gamma^t|$ less than $|\phi_\mathrm{Q}^t|$ at least by one hour, and a quarter of them even at least by two hours [Fig. 4(c); $P < 10^{-4}$ and Text S2]. These results suggest that $\bar{C}_{\mathrm{TF}\gamma}(\tau)$, as well as $\bar{C}_{\mathrm{TF}\gamma_\mathrm{p}}(\tau)$, is more likely to resemble $\bar{C}_\mathrm{TF}(\tau)$ in its phase than $\bar{C}_\mathrm{TFQ}(\tau)$ is.

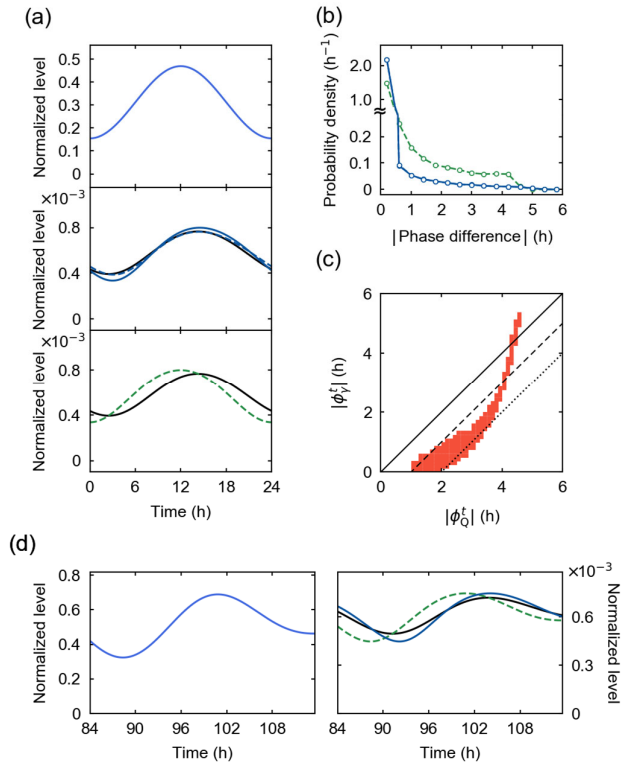

FIG. 4. TF–DNA interaction modeling. (a) Example time series of $\overline{A}_\mathrm{TF}(\tau)$ at the top, $\overline{C}_\mathrm{TF}(\tau)$ (black), $\bar{C}_{\mathrm{TF}\gamma}(\tau)$ (blue solid line), and $\bar{C}_{\mathrm{TF}\gamma_\mathrm{p}}(\tau)$ (blue dashed line) at the center, and $\overline{C}_\mathrm{TF}(\tau)$ (solid line) and $\bar{C}_\mathrm{TFQ}(\tau)$ (dashed line) at the bottom. The calculations are based on Eqs. (30), (31), (39), (46), and (52), and $t = k_\delta^{-1}\tau$ as defined in Sec. II.B. (b) Probability distributions of $|\phi_\gamma^t|$ (blue solid line), $|\phi_{\gamma_\mathrm{p}}^t|$ (blue dashed line), and $|\phi_\mathrm{Q}^t|$ (green dashed line) over randomly-sampled parameter sets in Table S3. Those of $|\phi_\gamma^t|$ and $|\phi_{\gamma_\mathrm{p}}^t|$ highly overlap and are not visually distinguishable here. (c) Scatter plot of $|\phi_\mathrm{Q}^t|$ and $|\phi_\gamma^t|$ when $|\phi_\mathrm{Q}^t|$ or $|\phi_\gamma^t|$ ≥1 h with randomly-sampled parameter sets in Table S3. A solid diagonal line corresponds to $|\phi_\gamma^t| = |\phi_\mathrm{Q}^t|$, a dashed diagonal line to $|\phi_\gamma^t| = |\phi_\mathrm{Q}^t| - 1\mathrm{h}$, and a dotted diagonal line to $|\phi_\gamma^t| = |\phi_\mathrm{Q}^t| - 2\mathrm{h}$. (d) When based on Eq. (53), example time series of $\overline{A}_\mathrm{TF}(\tau)$ on the left and $\overline{C}_\mathrm{TF}(\tau)$ (black solid line), $\bar{C}_{\mathrm{TF}\gamma}(\tau)$ (blue solid line), and $\bar{C}_\mathrm{TFQ}(\tau)$ (green dashed line) on the right. They were calculated in the same way as (a), except for the use of Eq. (53) instead of Eq. (52). For the detailed methods in (a)–(d) and the parameters in (a) and (d), refer to Text S2.

Unlike the cases of phases, we expect that the wave profiles predicted by $\bar{C}_{\mathrm{TF}\gamma}(\tau)$ and $\bar{C}_\mathrm{TFQ}(\tau)$ would be almost the same, with regards to Eq. (39). We examine this issue in a similar way to Sec. III.B: we measure similarity S_γ between the profiles of $\bar{C}_{\mathrm{TF}\gamma}(\tau)$ and $\bar{C}_\mathrm{TF}(\tau)$ after aligning their phases to the same (Text S2). Analogously, S_{γ_p} is defined for $\bar{C}_{\mathrm{TF}\gamma_\mathrm{p}}(\tau)$ and $\bar{C}_\mathrm{TF}(\tau)$, and S_Q for $\bar{C}_\mathrm{TFQ}(\tau)$ and $\bar{C}_\mathrm{TF}(\tau)$. S_γ, S_{γ_p}, and S_Q range from 0 to 1: the larger a value of S_γ, the more similar are the wave profiles of $\bar{C}_{\mathrm{TF}\gamma}(\tau)$ and $\bar{C}_\mathrm{TF}(\tau)$, and the same for the cases of S_{γ_p} and S_Q (Text S2). As anticipated, S_γ and S_Q take almost the same values as each other

(Spearman's $\rho = 0.94$ and $P < 10^{-4}$) and both are > 0.7 for the physiologically-relevant conditions (Text S2). Notably, S_{γ_p} even exceeds S_γ and S_Q in most cases ($> 99\%$) because of the more correct amplitude of $\bar{C}_{\mathrm{TF}\gamma_\mathrm{p}}(\tau)$ in Eq. (46).

To summarize, our revised MM rate law $\bar{C}_{\mathrm{TF}\gamma}(\tau)$ improves a phase approximation of $\bar{C}_\mathrm{TF}(\tau)$, while $\bar{C}_{\mathrm{TF}\gamma}(\tau)$ and $\bar{C}_\mathrm{TFQ}(\tau)$ exhibit very similar wave profiles. $\bar{C}_{\mathrm{TF}\gamma}(\tau)$ further improves to the form of $\bar{C}_{\mathrm{TF}\gamma_\mathrm{p}}(\tau)$. One may expect that the high accuracy of $\bar{C}_{\mathrm{TF}\gamma}(\tau)$ in the phases might be indicated by the range of the valid conditions of $\bar{C}_{\mathrm{TF}\gamma}(\tau)$ in Eqs. (41) and (42). In fact, most of our simulated conditions (92.0%) in Table S3 satisfy $\max_\tau[\varepsilon_\mathrm{TF}(\tau)] \leq 0.1$ and therefore only $\varepsilon_{\mathrm{TF}\gamma}(\tau)$ and $\varepsilon_\mathrm{TFQ}(\tau)$ in Eqs. (42) and (44) remain the key determinants of the validities of $\bar{C}_{\mathrm{TF}\gamma}(\tau)$ and $\bar{C}_\mathrm{TFQ}(\tau)$, respectively. Our analysis shows that $\max_\tau\left[\varepsilon_{\mathrm{TF}\gamma}(\tau)\right] \leq 0.1$ for 81.6% of the conditions, slightly more than the conditions (69.9%) with $\max_\tau\left[\varepsilon_\mathrm{TFQ}(\tau)\right] \leq 0.1$. Naturally, $\max_\tau\left[\varepsilon_{\mathrm{TF}\gamma}(\tau)\right]$ and $\max_\tau\left[\varepsilon_\mathrm{TFQ}(\tau)\right]$ strongly correlate with $\left|\phi_\gamma^t\right|$ and $\left|\phi_\mathrm{Q}^t\right|$, respectively (Spearman's $\rho = 0.69$ between $\max_\tau\left[\varepsilon_{\mathrm{TF}\gamma}(\tau)\right]$ and $\left|\phi_\gamma^t\right|$, and $\rho = 0.89$ between $\max_\tau\left[\varepsilon_\mathrm{TFQ}(\tau)\right]$ and $\left|\phi_\mathrm{Q}^t\right|$; $P < 10^{-4}$ and Text S2).

Although physiologically less relevant, the oscillatory TF level with irregular rhythmicity may provide another testbed for the approximating capability of $\bar{C}_{\mathrm{TF}\gamma}(\tau)$. Hence, instead of Eq. (52), we consider the following $\overline{A}_\mathrm{TF}(\tau)$ and numerically solve Eq. (30):

$$\overline{A}_\mathrm{TF}(\tau) = \frac{1}{N}\sum_{i=1}^{N}\overline{A}_{\max,i}\left\{1 - \frac{\alpha_{\mathrm{A},i}}{2}\left[1 + \cos\left(\frac{2\pi}{k_\delta T_{\mathrm{A},i}}\tau - \varphi_{\mathrm{A},i}\right)\right]\right\}, \quad (53)$$

We choose $N = 10$ and randomly select the other parameters from the ranges in Text S2. Even with such irregularity of the rhythms, $\bar{C}_{\mathrm{TF}\gamma}(\tau)$ is still found to improve the approximation of $\bar{C}_\mathrm{TF}(\tau)$ compared to $\bar{C}_\mathrm{TFQ}(\tau)$, as illustrated in Fig. 4(d).

D. Autogenous control

Our revised MM rate law offers a valuable analytical tool for the study of transient behaviors of biochemical systems, such as those of autogenously regulated systems where TFs regulate their own transcription. This autogenous control underlies cellular responses to various internal and external stimuli or signals [34,35]. We here explore the cases of positively and negatively autoregulated systems.

In the case of positive autoregulation, consider a scenario in Fig. 5(a) that proteins enhance their own transcription after homodimer formation and this dimer–promoter interaction is facilitated by inducer molecules. The protein production is hence governed by the following equations:

$$\frac{\mathrm{d}M(t)}{\mathrm{d}t} = \frac{s}{V} + (a_0 - s)C_\mathrm{TF}(t) - (b_0 + k_\mathrm{dlt})M(t), \quad (54)$$

$$\frac{\mathrm{d}A(t)}{\mathrm{d}t} = a_1 M(t) - (r_\mathrm{c} + k_\mathrm{dlt})A(t), \quad (55)$$

$$\frac{\mathrm{d}A_2(t)}{\mathrm{d}t} = \frac{k_\mathrm{a}}{2}[A(t) - 2A_2(t)]^2 - (k_\mathrm{d} + r_\mathrm{c} + k_\mathrm{dlt})A_2(t), \quad (56)$$

$$\frac{\mathrm{d}C_\mathrm{TF}(t)}{\mathrm{d}t} = \frac{\eta\hat{k}_\mathrm{TFa}}{V}A_2(t) - \left[k_\mathrm{TFd} + k_\mathrm{dlt} + \eta\hat{k}_\mathrm{TFa}A_2(t)\right]C_\mathrm{TF}(t). \quad (57)$$

Here, $M(t)$, $A(t)$, $A_2(t)$, and $C_\mathrm{TF}(t)$ are the total mRNA, protein, protein dimer, and promoter-binding dimer concentrations, respectively. Eqs. (56) and (57) are based on Eqs. (1) and (30), but modified for homodimerization and dilution with cell growth. s, a_0, and a_1 denote the basal and maximal transcription rates ($s \ll a_0$) and translation rate, respectively. b_0, r_c, and k_dlt denote the mRNA and protein degradation rates and cell growth-related dilution rate, respectively. k_a, k_d, and k_TFd denote the dimer association and dissociation rates and dimer–promoter dissociation rate, respectively. η is a dimensionless quantity, monotonically increasing with an inducer level. $\eta\hat{k}_\mathrm{TFa}$ and V correspond to k_a and V in Eqs. (28)–(30), respectively. We here assume that the promoter-binding dimers are neither dissociated to monomers nor degraded. To be precise, $-(r_\mathrm{c} + k_\mathrm{dlt})A(t)$ and $-(k_\mathrm{d} + r_\mathrm{c} +$

$k_{\mathrm{dlt}})A_2(t)$ in Eqs. (55) and (56) should be replaced by $-r_{\mathrm{c}}[A(t) - 2C_{\mathrm{TF}}(t)] - k_{\mathrm{dlt}}A(t)$ and $-(k_{\mathrm{d}} + r_{\mathrm{c}})[A_2(t) - C_{\mathrm{TF}}(t)] - k_{\mathrm{dlt}}A_2(t)$, respectively; however, this replacement does not much affect our simulation results, and thus we keep the original forms of Eqs. (55) and (56) for the straightforward approximation of the dimer concentration later.

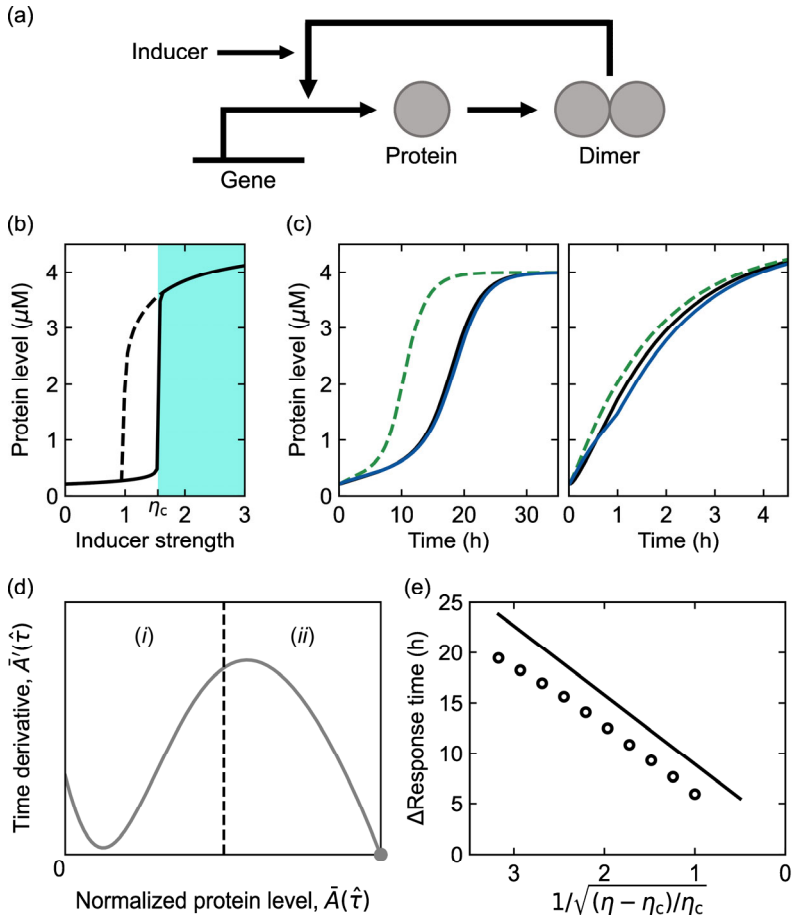

FIG. 5. Positive autoregulation and induction kinetics. (a) Protein production mechanism with positive autoregulation in the presence of inducers. (b) Bifurcation diagram of protein level $A(t)$ as a function of η (proxy for an inducer level) from Eqs. (54)–(57). The steady state is plotted as η increases (solid line) or decreases (dashed line). Acute induction can be simulated by a sudden change of $\eta = 0$ to $\eta > \eta_{\mathrm{c}}$ in the shaded area. (c) Time-series of $A(t)$ from the full model (black solid line), our revised MM rate law (blue solid line), and the tQSSA (green dashed line) upon acute induction at $t = 0$ with a small (left) or large (right) value of η ($\eta > \eta_{\mathrm{c}}$). The full model is based on Eqs. (54)–(57), or equivalently Eqs. (58)–(61), our revised MM rate law on Eqs. (59) and (63), and the tQSSA on Eqs. (59) and (62). (d) $\bar{A}'(\hat{\tau})$ as a function of $\bar{A}(\hat{\tau})$ from Eq. (65) when η is larger than but still close to η_{c}. The stable fixed point is indicated by a filled circle. A vertical dashed line splits (*i*) and (*ii*) ranges of $\bar{A}(\hat{\tau})$ defined in Sec. III.D. (e) The full model-to-tQSSA difference in their simulated (open circles) or estimated (solid line) protein response times as a function of $1/\sqrt{(\eta - \eta_{\mathrm{c}})/\eta_{\mathrm{c}}}$. The estimation is based on Eq. (75). For the detailed methods in (b)–(e), refer to Text S2.

As the simulated inducer level increases with η, Fig. 5(b) demonstrates that the initially low, steady-state protein level $[A(t)]$ undergoes an abrupt leap at a certain point $\eta = \eta_{\mathrm{c}}$ (Text S2). Right before this point, a bistable regime of the protein level exists and this bistability has previously been known for positive autoregulation with cooperativity [Fig. 5(b)] [34,36]. Upon acute induction by an $\eta = 0$ to $\eta > \eta_{\mathrm{c}}$ switch, the protein level grows over time towards a new steady state and this response becomes faster at larger η away from η_{c} of the infinite

response time [Fig. 5(c) and Text S2]. Still, the response is slower than under negative autoregulation of later focus, when protein steady states are similar in that comparison—the result consistent with the previous reports [34,35].

To analyze the induction kinetics in light of our revised MM rate law, we first rewrite Eqs. (54)–(57) as

$$\frac{\mathrm{d}\bar{M}(\hat{\tau})}{\mathrm{d}\hat{\tau}} = \sigma + (1-\sigma)\bar{\bar{C}}_{\mathrm{TF}}(\hat{\tau}) - B_0\bar{M}(\hat{\tau}), \quad (58)$$

$$\frac{\mathrm{d}\bar{A}(\hat{\tau})}{\mathrm{d}\hat{\tau}} = \bar{M}(\hat{\tau}) - \bar{A}(\hat{\tau}), \quad (59)$$

$$\frac{\mathrm{d}\bar{A}_2(\hat{\tau})}{\mathrm{d}\hat{\tau}} = R[\bar{A}(\hat{\tau}) - 2\bar{A}_2(\hat{\tau})]^2 - D\bar{A}_2(\hat{\tau}), \quad (60)$$

$$\frac{\mathrm{d}\bar{\bar{C}}_{\mathrm{TF}}(\hat{\tau})}{\mathrm{d}\hat{\tau}} = \eta P\bar{A}_2(\hat{\tau}) - [D_{\mathrm{TF}} + \eta P\bar{A}_2(\hat{\tau})]\bar{\bar{C}}_{\mathrm{TF}}(\hat{\tau}), \quad (61)$$

where all the variables and parameters are dimensionless as $\hat{\tau} \equiv (r_{\mathrm{c}} + k_{\mathrm{dlt}})t$, $\bar{M}(\hat{\tau}) \equiv (r_{\mathrm{c}} + k_{\mathrm{dlt}})a_0^{-1}VM(t)$, $\bar{A}(\hat{\tau}) \equiv (r_{\mathrm{c}} + k_{\mathrm{dlt}})^2(a_0a_1)^{-1}VA(t)$, $\bar{A}_2(\hat{\tau}) \equiv (r_{\mathrm{c}} + k_{\mathrm{dlt}})^2(a_0a_1)^{-1}VA_2(t)$, $\bar{\bar{C}}_{\mathrm{TF}}(\hat{\tau}) \equiv VC_{\mathrm{TF}}(t)$, $\sigma \equiv sa_0^{-1} \ll 1$, $B_0 \equiv (b_0 + k_{\mathrm{dlt}})(r_{\mathrm{c}} + k_{\mathrm{dlt}})^{-1}$, $R \equiv k_{\mathrm{a}}a_0a_1(2V)^{-1}(r_{\mathrm{c}} + k_{\mathrm{dlt}})^{-3}$, $D \equiv (k_{\mathrm{d}} + r_{\mathrm{c}} + k_{\mathrm{dlt}})(r_{\mathrm{c}} + k_{\mathrm{dlt}})^{-1}$, $P \equiv \hat{k}_{\mathrm{TFa}}a_0a_1V^{-1}(r_{\mathrm{c}} + k_{\mathrm{dlt}})^{-3}$, and $D_{\mathrm{TF}} \equiv (k_{\mathrm{TFd}} + k_{\mathrm{dlt}})(r_{\mathrm{c}} + k_{\mathrm{dlt}})^{-1}$.

Eqs. (60) and (61) are equivalent to Eqs. (2) and (30) with the mapping of $D\hat{\tau}$, $4RD^{-1}\bar{A}_2(\hat{\tau})$, and $2RD^{-1}\bar{A}(\hat{\tau})$ in Eq. (60) to τ, $\bar{C}(\tau)$, and both $\bar{A}(\tau)$ and $\bar{B}(\tau)$ in Eq. (2) and that of $D_{\mathrm{TF}}\hat{\tau}$, $\bar{\bar{C}}_{\mathrm{TF}}(\hat{\tau})$, and $\eta PD_{\mathrm{TF}}^{-1}\bar{A}_2(\hat{\tau})$ in Eq. (61) to τ, $KV\bar{C}_{\mathrm{TF}}(\tau)$, and $\bar{A}_{\mathrm{TF}}(\tau)$ in Eq. (30), respectively. From Eqs. (5) and (31), the tQSSA-based model then comprises Eq. (59) and this equation:

$$\frac{\mathrm{d}\bar{M}(\hat{\tau})}{\mathrm{d}\hat{\tau}} = \sigma + (1-\sigma)\frac{\eta PD_{\mathrm{TF}}^{-1}\bar{A}_{2\mathrm{tQ}}(\hat{\tau})}{1+\eta PD_{\mathrm{TF}}^{-1}\bar{A}_{2\mathrm{tQ}}(\hat{\tau})} - B_0\bar{M}(\hat{\tau}), \quad (62)$$

where $\bar{A}_{2\mathrm{tQ}}(\hat{\tau}) \equiv \left[\kappa + \bar{A}(\hat{\tau}) - \sqrt{\bar{\Delta}_{\mathrm{tQ}}(\hat{\tau})}\right]/2$ with $\bar{\Delta}_{\mathrm{tQ}}(\hat{\tau}) \equiv \kappa[\kappa + 2\bar{A}(\hat{\tau})]$ and $\kappa \equiv D/(4R)$. Although the sQSSA-based model can also be obtained using the Padé approximant for $\bar{A}_{2\mathrm{tQ}}(\hat{\tau})$, we do not consider it now because of the tQSSA's higher accuracy than the sQSSA's. On the other hand, from Eqs. (18) and (39), our revised MM rate law gives rise to a model with Eq. (59) and the following equation:

$$\frac{\mathrm{d}\bar{M}(\hat{\tau})}{\mathrm{d}\hat{\tau}} = \sigma + (1-\sigma)\frac{\eta PD_{\mathrm{TF}}^{-1}\bar{A}_{2\gamma}\left[\hat{\tau} - \frac{1}{D_{\mathrm{TF}}+\eta P\bar{A}_{2\gamma}(\hat{\tau})}\right]}{1+\eta PD_{\mathrm{TF}}^{-1}\bar{A}_{2\gamma}\left[\hat{\tau} - \frac{1}{D_{\mathrm{TF}}+\eta P\bar{A}_{2\gamma}(\hat{\tau})}\right]} - B_0\bar{M}(\hat{\tau}), \quad (63)$$

where $\bar{A}_{2\gamma}(\hat{\tau}) \equiv \min\left\{\bar{A}_{2\mathrm{tQ}}\left[\hat{\tau} - R^{-1}\bar{\Delta}_{\mathrm{tQ}}^{-1/2}(\hat{\tau})/4\right], \bar{A}(\hat{\tau})/2\right\}$ with the aforementioned $\bar{A}_{2\mathrm{tQ}}(\hat{\tau})$ and $\bar{\Delta}_{\mathrm{tQ}}(\hat{\tau})$.

When there is a sudden $\eta = 0$ to $\eta > \eta_{\mathrm{c}}$ change, the induced protein time-series can be compared between the full model [Eqs. (58)–(61)], our revised rate law [Eqs. (59) and (63)], and the tQSSA [Eqs. (59) and (62)]. These three cases with a common parameter set have the inherently same steady states at the end, but may differ in their transient behaviors. Across physiologically-relevant conditions in Table S5, we found that the revised rate law tends to better agree with the full model in the protein response time than the tQSSA ($P < 10^{-4}$ and Text S2. In this study, the response time is defined as the time taken for a protein level to reach 90% of its steady state). This performance difference between ours and the tQSSA is evident at small η values as exemplified by Fig. 5(c). This observation prompts us to seek the analytical expression of the response time with our revised rate law and compare it with the tQSSA's.

Consider this condition:

$$\bar{A}(\hat{\tau}) \ll \kappa \text{ and } B_0 \gg 1, \quad (64)$$

which allow us to take $\bar{A}_{2\mathrm{tQ}}(\hat{\tau}) \approx \bar{A}^2(\hat{\tau})/(4\kappa)$, $R^{-1}\bar{\Delta}_{\mathrm{tQ}}^{-1/2}(\hat{\tau})/4 \approx 1/D$, and an instantly-acclimating mRNA level with $\bar{M}'(\hat{\tau}) \approx 0$ in Eqs. (62) and (63). Plugging them in Eq. (59) leads to

$$\frac{\mathrm{d}\bar{A}(\hat{\tau})}{\mathrm{d}\hat{\tau}} \approx \frac{\sigma}{B_0} + \frac{1-\sigma}{B_0}\cdot\frac{\left(\frac{\eta P}{4\kappa D_{\mathrm{TF}}}\right)\bar{A}^2(\hat{\tau})}{1+\left(\frac{\eta P}{4\kappa D_{\mathrm{TF}}}\right)\bar{A}^2(\hat{\tau})} - \bar{A}(\hat{\tau}), \quad (65)$$

$$\frac{\mathrm{d}\bar{A}(\hat{\tau})}{\mathrm{d}\hat{\tau}} \approx \frac{\sigma}{B_0} + \frac{1-\sigma}{B_0} \cdot \frac{\left(\frac{\eta P}{4\kappa D_{\mathrm{TF}}}\right)\bar{A}^2\left[\hat{\tau} - \frac{D_{\mathrm{TF}}^{-1}}{1+\left(\frac{\eta P}{4\kappa D_{\mathrm{TF}}}\right)\bar{A}^2\left(\hat{\tau}-\frac{1}{D}\right)} - \frac{1}{D}\right]}{1+\left(\frac{\eta P}{4\kappa D_{\mathrm{TF}}}\right)\bar{A}^2\left[\hat{\tau} - \frac{D_{\mathrm{TF}}^{-1}}{1+\left(\frac{\eta P}{4\kappa D_{\mathrm{TF}}}\right)\bar{A}^2\left(\hat{\tau}-\frac{1}{D}\right)} - \frac{1}{D}\right]} - \bar{A}(\hat{\tau}). \qquad (66)$$

Eqs. (65) and (66) come from the tQSSA and our revised rate law, respectively. The sQSSA in the condition of Eq. (64) ends up at Eq. (65) too, and thus we will refer to Eq. (65) just as conventional, rather than the tQSSA- or sQSSA-specific. Because $\bar{A}(\hat{\tau}) \to \sigma/B_0$ at the steady state at $\eta = 0$ and the above $\sigma \ll 1$ and $B_0 \gg 1$ ensure $\sigma/B_0 \ll 1$, we treat the initial $\bar{A}(\hat{\tau})$ as ~ 0 when η switches from 0 to $> \eta_{\mathrm{c}}$. To estimate the relevant protein response time, we consider two different ranges of $\bar{A}(\hat{\tau})$ over its growth: (*i*) $0 \lesssim \bar{A}(\hat{\tau}) < 2\sqrt{\kappa D_{\mathrm{TF}}\eta^{-1}P^{-1}}$ and (*ii*) $2\sqrt{\kappa D_{\mathrm{TF}}\eta^{-1}P^{-1}} \leq \bar{A}(\hat{\tau}) < \bar{A}_*$ where $\bar{A}_*$ is the steady state of $\bar{A}(\hat{\tau})$. The phase portrait of Eq. (65) in (*i*) and (*ii*) is illustrated by Fig. 5(d). For (*i*) and (*ii*), Eq. (65) respectively reduces to

$$\frac{\mathrm{d}\bar{A}(\hat{\tau})}{\mathrm{d}\hat{\tau}} \approx c + a\bar{A}^2(\hat{\tau}) - \bar{A}(\hat{\tau}) \text{ and } \frac{\mathrm{d}\bar{A}(\hat{\tau})}{\mathrm{d}\hat{\tau}} \approx \frac{1}{B_0} - \bar{A}(\hat{\tau}), \quad (67)$$

where $a \equiv \eta P(1-\sigma)/(4\kappa B_0 D_{\mathrm{TF}})$ and $c \equiv \sigma/B_0$. The dimensionless form of the response time based on $\hat{\tau}$ is thus approximated by

$$[\hat{\tau}]_0^{\bar{A}(\hat{\tau})=\zeta\bar{A}_*} = \int_0^{2\sqrt{\frac{\kappa D_{\mathrm{TF}}}{\eta P}}} \frac{\mathrm{d}\bar{A}(\hat{\tau})}{\bar{A}'(\hat{\tau})} + \int_{2\sqrt{\frac{\kappa D_{\mathrm{TF}}}{\eta P}}}^{\zeta\bar{A}_*} \frac{\mathrm{d}\bar{A}(\hat{\tau})}{\bar{A}'(\hat{\tau})}$$

$$\approx \frac{2}{\sqrt{\frac{\eta-\eta_*}{\eta_*}}}\left\{\arctan\left[\frac{\sqrt{\frac{(1-\sigma)\eta}{\sigma\eta_*}}-1}{\sqrt{\frac{\eta-\eta_*}{\eta_*}}}\right] + \arctan\left(\frac{1}{\sqrt{\frac{\eta-\eta_*}{\eta_*}}}\right)\right\} + \ln\left[\frac{1-2\sqrt{\frac{(1-\sigma)\sigma\eta_*}{\eta}}}{1-\zeta}\right], \quad (68)$$

where $\bar{A}_* \approx 1/B_0$ from Eq. (67), $\zeta = 0.9$ by our definition of the response time, and

$$\eta_* \equiv \frac{B_0^2 \kappa D_{\mathrm{TF}}}{P\sigma(1-\sigma)}. \quad (69)$$

When $\eta \to \eta_*$, the response time in Eq. (68) diverges. η_* does approximate the transition point, i.e., $\eta_{\mathrm{c}} \approx \eta_*$. Applying this fact and $\sigma \ll 1$ to Eq. (68) for $\eta \to \eta_{\mathrm{c}}$ informs the conventional response time near the transition point, as follows:

$$\frac{2\pi}{\sqrt{\frac{\eta-\eta_{\mathrm{c}}}{\eta_{\mathrm{c}}}}} + \ln\left(\frac{1-2\sqrt{\sigma}}{1-\zeta}\right). \quad (70)$$

Indeed, this estimate tends to match the tQSSA model simulation with Eqs. (59) and (62) under the condition of Eq. (64) [9.6 ± 9.0% relative error (avg. ± s.d. in simulated conditions); $P < 10^{-4}$ and Text S2].

Meanwhile, regarding our revised rate law, Eq. (66) in (*i*) reduces to

$$\frac{\mathrm{d}\bar{A}(\hat{\tau})}{\mathrm{d}\hat{\tau}} \approx c + a\bar{A}^2\left(\hat{\tau} - \frac{1}{D_{\mathrm{TF}}} - \frac{1}{D}\right) - \bar{A}(\hat{\tau}), \quad (71)$$

where a and c are the same as Eq. (67). Roughly, $\bar{A}\left(\hat{\tau} - D_{\mathrm{TF}}^{-1} - D^{-1}\right) > 0$ only if $\bar{A}(\hat{\tau}) > \bar{A}_{\min} \equiv c\left[1 - \left(1 + D_{\mathrm{TF}}^{-1} + D^{-1}\right)^{-1}\right]$, because $\bar{A}\left(\hat{\tau} - D_{\mathrm{TF}}^{-1} - D^{-1}\right) \approx \bar{A}(\hat{\tau}) - \left(D_{\mathrm{TF}}^{-1} + D^{-1}\right)\bar{A}'(\hat{\tau})$ and $\bar{A}'(\hat{\tau})$ is given by

$$\frac{\mathrm{d}\bar{A}(\hat{\tau})}{\mathrm{d}\hat{\tau}} \approx \frac{2a\left(D_{\mathrm{TF}}^{-1}+D^{-1}\right)\bar{A}(\hat{\tau})+1-\sqrt{4a\left(D_{\mathrm{TF}}^{-1}+D^{-1}\right)^2\left[\left(1+\frac{1}{D_{\mathrm{TF}}^{-1}+D^{-1}}\right)\bar{A}(\hat{\tau})-c\right]+1}}{2a\left(D_{\mathrm{TF}}^{-1}+D^{-1}\right)^2}. \quad (72)$$

$\bar{A}'(\hat{\tau})$ above is the solution of $a\left(D_{\mathrm{TF}}^{-1} + D^{-1}\right)^2[\bar{A}'(\hat{\tau})]^2 - \left[2a\left(D_{\mathrm{TF}}^{-1} + D^{-1}\right)\bar{A}(\hat{\tau}) + 1\right]\bar{A}'(\hat{\tau}) + a\bar{A}^2(\hat{\tau}) - \bar{A}(\hat{\tau}) + c \approx 0$. It comes from Eq. (71) and $\bar{A}^2\left(\hat{\tau} - D_{\mathrm{TF}}^{-1} - D^{-1}\right) \approx \bar{A}^2(\hat{\tau}) - 2\left(D_{\mathrm{TF}}^{-1} + D^{-1}\right)\bar{A}(\hat{\tau})\bar{A}'(\hat{\tau}) + \left(D_{\mathrm{TF}}^{-1} + D^{-1}\right)^2[\bar{A}'(\hat{\tau})]^2$ as $\bar{A}''(\hat{\tau}) \sim 0$ in (*i*) when η is not too larger than η_{c} so that $\bar{A}(\hat{\tau})$ exhibits prolonged slow growth. Apart from Eq. (72) for $\bar{A}(\hat{\tau}) > \bar{A}_{\min}$ in (*i*), we obtain $\bar{A}'(\hat{\tau}) \approx c - \bar{A}(\hat{\tau})$ for $\bar{A}(\hat{\tau}) \leq \bar{A}_{\min}$ by setting $\bar{A}\left(\hat{\tau} - D_{\mathrm{TF}}^{-1} - D^{-1}\right)$ in Eq. (71) as ~ 0. $\bar{A}'(\hat{\tau})$ in (*ii*) remains the same as the second equation in Eq. (67). Therefore, the response time takes this form:

$$[\hat{\tau}]_0^{\bar{A}(\hat{\tau})=\zeta\bar{A}_*} = \int_0^{\bar{A}_{\min}} \frac{\mathrm{d}\bar{A}(\hat{\tau})}{\bar{A}'(\hat{\tau})} + \int_{\bar{A}_{\min}}^{2\sqrt{\frac{\kappa D_{\mathrm{TF}}}{\eta P}}} \frac{\mathrm{d}\bar{A}(\hat{\tau})}{\bar{A}'(\hat{\tau})} + \int_{2\sqrt{\frac{\kappa D_{\mathrm{TF}}}{\eta P}}}^{\zeta\bar{A}_*} \frac{\mathrm{d}\bar{A}(\hat{\tau})}{\bar{A}'(\hat{\tau})}$$

$$\approx \ln\left(1+\frac{1}{D_{\mathrm{TF}}}+\frac{1}{D}\right)+\left(\frac{1}{D_{\mathrm{TF}}}+\frac{1}{D}\right)\ln\left\{1+\frac{DD_{\mathrm{TF}}(u-1)[DD_{\mathrm{TF}}(u-1)-2(D+D_{\mathrm{TF}})]}{(D+D_{\mathrm{TF}})^2\frac{\eta}{\eta_*}}\right\}$$

$$+\frac{2}{\sqrt{\frac{\eta-\eta_*}{\eta_*}}}\left(1+\frac{1}{D_{\mathrm{TF}}}+\frac{1}{D}\right)\left\{\arctan\left[\frac{DD_{\mathrm{TF}}(u-1)-D-D_{\mathrm{TF}}}{(D+D_{\mathrm{TF}})\sqrt{\frac{\eta-\eta_*}{\eta_*}}}\right]+\arctan\left(\frac{1}{\sqrt{\frac{\eta-\eta_*}{\eta_*}}}\right)\right\}+\ln\left[\frac{1-2\sqrt{\frac{(1-\sigma)\sigma\eta_*}{\eta}}}{1-\zeta}\right], \quad (73)$$

where $u \equiv \sqrt{\sqrt{\eta\eta_*^{-1}}(D_{\mathrm{TF}}^{-1}+D^{-1})^2\left\{2[1+(D_{\mathrm{TF}}^{-1}+D^{-1})^{-1}]\sqrt{\sigma^{-1}(1-\sigma)}-\sqrt{\eta\eta_*^{-1}}\right\}+1}$ and the other notations are the same as Eq. (68).

In a similar fashion to the previous trial, $\eta_{\mathrm{c}} \approx \eta_*$ and $\sigma \ll 1$ get into Eq. (73) with $\eta \to \eta_{\mathrm{c}}$, and then our revised rate law predicts the near-transition response time as

$$\frac{2\pi}{\sqrt{\frac{\eta-\eta_{\mathrm{c}}}{\eta_{\mathrm{c}}}}}\left(1+\frac{1}{D_{\mathrm{TF}}}+\frac{1}{D}\right)+\ln\left(\frac{1-2\sqrt{\sigma}}{1-\zeta}\right)+\ln\left(1+\frac{1}{D_{\mathrm{TF}}}+\frac{1}{D}\right)$$
$$+\left(\frac{1}{D_{\mathrm{TF}}}+\frac{1}{D}\right)\ln\left\{1+\frac{DD_{\mathrm{TF}}(\bar{u}-1)[DD_{\mathrm{TF}}(\bar{u}-1)-2(D+D_{\mathrm{TF}})]}{(D+D_{\mathrm{TF}})^2}\right\}, \quad (74)$$

where $\bar{u} \equiv \sqrt{(D_{\mathrm{TF}}^{-1}+D^{-1})^2\{2[1+(D_{\mathrm{TF}}^{-1}+D^{-1})^{-1}]\sigma^{-1/2}-1\}+1}$. Remarkably, the full model simulation with Eqs. (58)–(61) under the condition Eq. (64) does support the above predicted response time [14.3 ± 12.6% relative error (avg. ± s.d. in simulated conditions); $P < 10^{-4}$ and Text S2]. Although the predicted response time looks complex in its form, only the first term $2\pi\left(1+D_{\mathrm{TF}}^{-1}+D^{-1}\right)/\sqrt{(\eta-\eta_{\mathrm{c}})/\eta_{\mathrm{c}}}$ becomes dominating as $\eta \to \eta_{\mathrm{c}}$. $D_{\mathrm{TF}}^{-1}+D^{-1}$ here represents the unique feature of our prediction, as will be discussed below.

Subtracting Eq. (70) from Eq. (74) reveals that our predicted response time is longer than the conventional one by

$$\frac{2\pi}{\sqrt{\frac{\eta-\eta_{\mathrm{c}}}{\eta_{\mathrm{c}}}}}\left(\frac{1}{D_{\mathrm{TF}}}+\frac{1}{D}\right)+\ln\left(1+\frac{1}{D_{\mathrm{TF}}}+\frac{1}{D}\right)+\left(\frac{1}{D_{\mathrm{TF}}}+\frac{1}{D}\right)\ln\left\{1+\frac{DD_{\mathrm{TF}}(\bar{u}-1)[DD_{\mathrm{TF}}(\bar{u}-1)-2(D+D_{\mathrm{TF}})]}{(D+D_{\mathrm{TF}})^2}\right\}. \quad (75)$$

Notably, this time difference vanishes as $D_{\mathrm{TF}}^{-1}+D^{-1} \to 0$. Because D^{-1} and D_{TF}^{-1} are proportional to the effective time delays in dimer formation and dimer–promoter association, respectively, the total delay $D_{\mathrm{TF}}^{-1}+D^{-1}$ is responsible for a relatively retarded response in our prediction. Strikingly, the time difference indefinitely grows as η decreases towards η_{c}, as a linear function of $1/\sqrt{(\eta-\eta_{\mathrm{c}})/\eta_{\mathrm{c}}}$. This prediction provides another means to test our theory, and readily accounts for the tQSSA's underestimation of the response time at small η in Fig. 5(c). Consistent with the prediction, the full model simulation always shows a longer response time than the tQSSA model simulation and the difference is linearly scaled to $1/\sqrt{(\eta-\eta_{\mathrm{c}})/\eta_{\mathrm{c}}}$ as exemplified by Fig. 5(e) ($R^2 > 0.98$ in simulated conditions and Text S2). Moreover, its predicted slope against $1/\sqrt{(\eta-\eta_{\mathrm{c}})/\eta_{\mathrm{c}}}$ [i.e., 2π ($6.28\cdots$) multiplied by $D_{\mathrm{TF}}^{-1}+D^{-1}$] is comparable with the simulation results [7.3 ± 0.3 (avg. ± s.d. in simulated conditions) multiplied by $D_{\mathrm{TF}}^{-1}+D^{-1}$; see Text S2]. The agreement of these nontrivial predictions with the numerical simulation results proves the validity of our approach. At the same time, we raise a caution against the conventional approach, which severely underestimates the near-transition response time, e.g., by a few tens of hours in the case of Fig. 5(e). Lastly, note that the analytical forms of the response times and their difference in Eqs. (68), (70), (73)–(75) are based on $\hat{\tau}$, and we thus divided them by $r_{\mathrm{c}}+k_{\mathrm{dlt}}$ for their actual values.

Next, we move to the case of negative autoregulation. Imagine that proteins repress their own transcription after homodimer formation and this dimer–promoter interaction is inhibited by inducer molecules, as in Fig. 6(a). In fact, the homodimerization itself is not an essential factor of our main results later, but considered for a fair comparison between this system and the above positive autoregulation case. The protein production kinetics is described by the following equations and Eqs. (55) and (56):

$$\frac{\mathrm{d}M(t)}{\mathrm{d}t} = \frac{s}{V} + (a_0 - s)\left[\frac{1}{V} - C_{\mathrm{TF}}(t)\right] - (b_0 + k_{\mathrm{dlt}})M(t), \quad (76)$$

$$\frac{\mathrm{d}C_{\mathrm{TF}}(t)}{\mathrm{d}t} = \frac{\hat{k}_{\mathrm{TFa}}}{\eta V}A_2(t) - \left[k_{\mathrm{TFd}} + k_{\mathrm{dlt}} + \frac{\hat{k}_{\mathrm{TFa}}}{\eta}A_2(t)\right]C_{\mathrm{TF}}(t), \quad (77)$$

where all the variables and parameters are the same as Eqs. (54) and (57) and $\hat{k}_{\mathrm{TFa}}/\eta$ corresponds to k_{a} in Eqs. (28)–(30). As the simulated inducer level increases with η, Fig. 6(b) demonstrates that the steady-state protein level $[A(t)]$ increases, yet does not show a discrete transition like the previous positive regulation's (Text S2). Upon acute induction by an $\eta = 0$ to $\eta > 0$ switch, the protein level grows to the new steady state over time and this response becomes slower at larger η [Fig. 6(c) and Text S2]. Still, the response is speedier than in the positive regulation case, when the protein steady states are similar in that comparison—consistent with the previous finding of the beneficial effect of negative autoregulation [35].

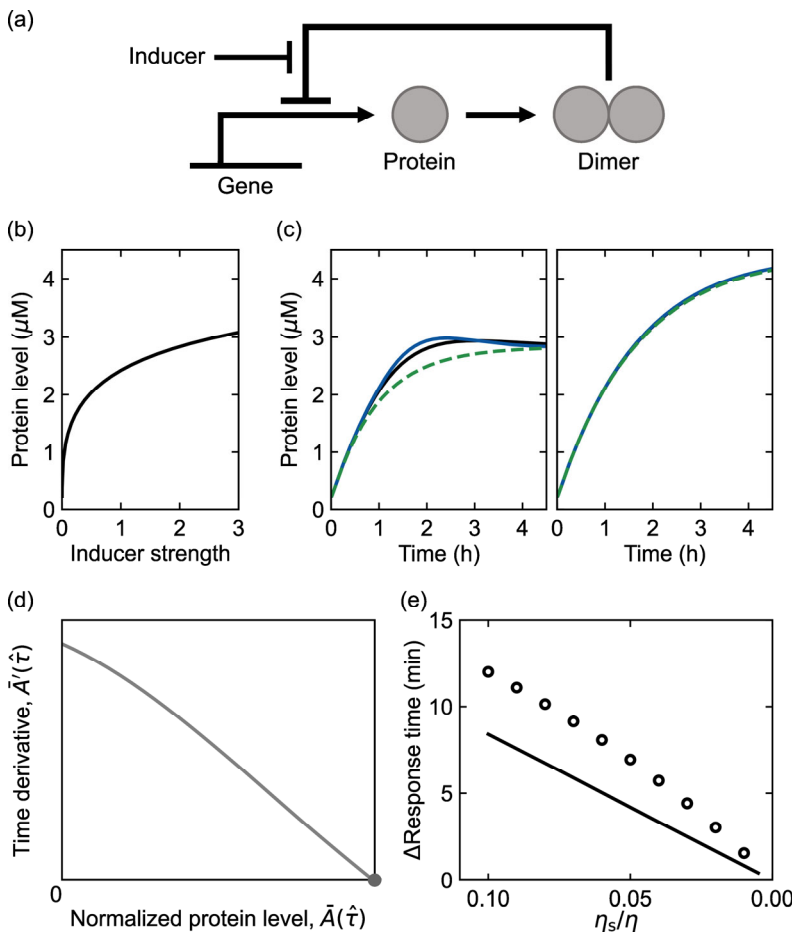

FIG. 6. Negative autoregulation and induction kinetics. (a) Protein production mechanism with negative autoregulation in the presence of inducers. (b) Bifurcation diagram of protein level $A(t)$ as a function of η (proxy for an inducer level) from Eqs. (55), (56), (76), and (77). (c) Time-series of $A(t)$ from the full model (black solid line), our revised MM rate law (blue solid line), and the tQSSA (green dashed line) with a change of $\eta = 0$ to a small (left) or large (right) value of $\eta > 0$ at $t = 0$. The full model is based on Eqs. (55), (56), (76), and (77), or equivalently Eqs. (59), (60), (78), and (79), our revised MM rate law

on Eqs. (59) and (81), and the tQSSA on Eqs. (59) and (80). (d) $\bar{A}'(\hat{\tau})$ as a function of $\bar{A}(\hat{\tau})$ in Eq. (82) for $\eta > 0$. The stable fixed point is indicated by a filled circle. (e) The tQSSA-to-full model difference in the simulated (open circles) or estimated (solid line) protein response times as a function of η_s/η for $\eta \gg \eta_s$. The estimation is based on Eq. (90). For the detailed methods in (b)–(e), refer to Text S2. The η values in (c) were chosen for the similar steady states to Fig. 5(c).

Adopting the dimensionless variables and parameters in Eqs. (58) and (61), we rewrite Eqs. (76) and (77) as

$$\frac{\mathrm{d}\bar{M}(\hat{\tau})}{\mathrm{d}\hat{\tau}} = \sigma + (1-\sigma)\left[1 - \bar{\bar{C}}_{\mathrm{TF}}(\hat{\tau})\right] - B_0\bar{M}(\hat{\tau}), \quad (78)$$

$$\frac{\mathrm{d}\bar{\bar{C}}_{\mathrm{TF}}(\hat{\tau})}{\mathrm{d}\hat{\tau}} = \frac{P}{\eta}\bar{A}_2(\hat{\tau}) - \left[D_{\mathrm{TF}} + \frac{P}{\eta}\bar{A}_2(\hat{\tau})\right]\bar{\bar{C}}_{\mathrm{TF}}(\hat{\tau}). \quad (79)$$

Eq. (79) is equivalent to Eq. (30) with the mapping of $D_{\mathrm{TF}}\hat{\tau}$, $\bar{\bar{C}}_{\mathrm{TF}}(\hat{\tau})$, and $P\eta^{-1}D_{\mathrm{TF}}^{-1}\bar{A}_2(\hat{\tau})$ to τ, $KV\bar{C}_{\mathrm{TF}}(\tau)$, and $\bar{A}_{\mathrm{TF}}(\tau)$, respectively. Therefore, based on the same procedure as the positive regulation case, we obtain the tQSSA-based model with Eq. (59) and the following equation:

$$\frac{\mathrm{d}\bar{M}(\hat{\tau})}{\mathrm{d}\hat{\tau}} = \sigma + \frac{(1-\sigma)\eta}{\eta + PD_{\mathrm{TF}}^{-1}\bar{A}_{2\mathrm{tQ}}(\hat{\tau})} - B_0\bar{M}(\hat{\tau}). \quad (80)$$

Likewise, our revised rate law leads to the model with Eq. (59) and the following equation:

$$\frac{\mathrm{d}\bar{M}(\hat{\tau})}{\mathrm{d}\hat{\tau}} = \sigma + \frac{(1-\sigma)\eta}{\eta + PD_{\mathrm{TF}}^{-1}\bar{A}_{2\gamma}\left[\hat{\tau} - \frac{\eta}{\eta D_{\mathrm{TF}} + P\bar{A}_{2\gamma}(\hat{\tau})}\right]} - B_0\bar{M}(\hat{\tau}). \quad (81)$$

$\bar{A}_{2\mathrm{tQ}}(\hat{\tau})$ and $\bar{A}_{2\gamma}(\hat{\tau})$ in Eqs. (80) and (81) are defined as in Eqs. (62) and (63).

When there is a sudden $\eta = 0$ to $\eta > 0$ change, the response time of the induced protein can be compared between the full model [Eqs. (59), (60), (78), and (79)], the revised rate law [Eqs. (59) and (81)], and the tQSSA [Eqs. (59) and (80)]. Across physiologically-relevant conditions in Table S5, we found that the revised rate law tends to better agree with the full model in the response time than the tQSSA, especially for small η values as exemplified by Fig. 6(c) [$P < 10^{-4}$ and Text S2. In Fig. 6(c) (left), the revised rate law even reproduces an overshoot in the protein level, whereas the tQSSA does not]. Like the positive regulation case, we will try the analytical formulation of the response times with our revised rate law and the tQSSA.

We assume Eq. (64) for Eqs. (59), (80), and (81) and obtain the following expressions with a notation $\eta_s \equiv P/(4\kappa D_{\mathrm{TF}}B_0^2)$:

$$\frac{\mathrm{d}\bar{A}(\hat{\tau})}{\mathrm{d}\hat{\tau}} \approx \frac{\sigma}{B_0} + \frac{1-\sigma}{B_0}\cdot\frac{1}{1+\frac{\eta_s}{\eta}B_0^2\bar{A}^2(\hat{\tau})} - \bar{A}(\hat{\tau}), \quad (82)$$

$$\frac{\mathrm{d}\bar{A}(\hat{\tau})}{\mathrm{d}\hat{\tau}} \approx \frac{\sigma}{B_0} + \frac{1-\sigma}{B_0}\cdot\frac{1}{1+\frac{\eta_s}{\eta}B_0^2\bar{A}^2\left[\hat{\tau} - \frac{D_{\mathrm{TF}}^{-1}}{1+\frac{\eta_s}{\eta}B_0^2\bar{A}^2\left(\hat{\tau}-\frac{1}{D}\right)} - \frac{1}{D}\right]} - \bar{A}(\hat{\tau}). \quad (83)$$

Eqs. (82) and (83) pertain to the tQSSA and our revised rate law, respectively. Because the sQSSA also ends up at Eq. (82) under Eq. (64), we will just refer to Eq. (82) as conventional, rather than the tQSSA- or sQSSA-specific. The phase portrait of Eq. (82) in Fig. 6(d) suggests that the closer to the steady state, the more rate-limiting in the protein response process. We therefore focus on the late-stage dynamics and assume

$$\bar{A}(\hat{\tau}) \approx \bar{A}_* - \epsilon e^{-\lambda(\hat{\tau}-\hat{\tau}_0)}, \quad (84)$$

where $\bar{A}_*$ is the steady state of $\bar{A}(\hat{\tau})$, λ and ϵ are positive constants, and $\hat{\tau}_0$ denotes the initial point of $\hat{\tau}$. Eq. (84) would work for large η without an overshoot in $\bar{A}(\hat{\tau})$. We first set $\bar{A}^2(\hat{\tau} - D^{-1})$ in Eq. (83) as $\sim\bar{A}_*^2$ and then apply Eq. (84) to Eq. (83). Consequently,

$$\epsilon\lambda e^{-\lambda(\hat{\tau}-\hat{\tau}_0)} \approx \frac{\sigma}{B_0} + \frac{1-\sigma}{B_0}\cdot\frac{1}{1+\frac{\eta_s}{\eta}B_0^2\left[\bar{A}_* - \epsilon e^{-\lambda(\hat{\tau}-\hat{\tau}_{\mathrm{d}}-\hat{\tau}_0)}\right]^2} + \epsilon e^{-\lambda(\hat{\tau}-\hat{\tau}_0)} - \bar{A}_*, \quad (85)$$

where $\hat{\tau}_{\mathrm{d}} \equiv D_{\mathrm{TF}}^{-1}[1 + \eta^{-1}\eta_s B_0^2\bar{A}_*^2]^{-1} + D^{-1}$. The Taylor expansion of Eq. (85) up to $O(\epsilon)$ gives rise to

$$\frac{2\eta_s B_0\bar{A}_*(1-\sigma)}{\eta\left(1+\frac{\eta_s}{\eta}B_0^2\bar{A}_*^2\right)^2}e^{\lambda\hat{\tau}_{\mathrm{d}}} - \lambda + 1 \approx 0. \quad (86)$$

The use of relation $e^x \geq 1 + x$ for Eq. (86) with $x = \lambda\hat{\tau}_{\mathrm{d}}$ leads to

$$\lambda \gtrsim \frac{\eta\left(1+\frac{\eta_s}{\eta}B_0^2\bar{A}_*^2\right)^2+2\eta_s B_0\bar{A}_*(1-\sigma)}{\eta\left(1+\frac{\eta_s}{\eta}B_0^2\bar{A}_*^2\right)^2-2\hat{\tau}_d\eta_s B_0\bar{A}_*(1-\sigma)}. \quad (87)$$

In a similar manner to the positive regulation case, we treat the initial $\bar{A}(\hat{\tau})$ as ~ 0. Compatibly, we treat $\bar{A}(\hat{\tau}-\hat{\tau}_d)$ as ~ 0 for $\hat{\tau} \leq \hat{\tau}_0 + \hat{\tau}_d$, as well. In that time period, $\bar{A}'(\hat{\tau}) \approx B_0^{-1} - \bar{A}(\hat{\tau})$ from the modified Eq. (83), and therefore $\bar{A}(\hat{\tau}_0+\hat{\tau}_d) \approx B_0^{-1}\left(1-e^{-\hat{\tau}_d}\right)$. For the continuity of this result with Eq. (84) at $\hat{\tau} \to \hat{\tau}_0 + \hat{\tau}_d$, it should be satisfied that $\epsilon \approx B_0^{-1}e^{(\lambda-1)\hat{\tau}_d} - (B_0^{-1} - \bar{A}_*)e^{\lambda\hat{\tau}_d}$. With this form of ϵ and the above-mentioned ζ, we solve Eq. (84) for $\hat{\tau} - \hat{\tau}_0$ when $\bar{A}(\hat{\tau}) = \zeta\bar{A}_*$, and this value of $\hat{\tau} - \hat{\tau}_0$ is the estimated response time in a dimensionless form. For simplicity, if one focuses on the case of $\eta \gg \eta_s$, $\bar{A}_* \approx B_0^{-1}$ from Eq. (82) or (83). Combining the current procedure with the relation in Eq. (87) predicts the upper limit of the response time based on our revised rate law, as follows:

$$\ln\left(\frac{1}{1-\zeta}\right) - 2(1-\sigma)\left(1+\frac{1}{D_{\mathrm{TF}}}+\frac{1}{D}\right)\left[\ln\left(\frac{1}{1-\zeta}\right)-\frac{1}{D_{\mathrm{TF}}}-\frac{1}{D}\right]\frac{\eta_s}{\eta}, \quad (88)$$

which is obtained by the Taylor expansion up to $O(\eta_s/\eta)$ for $\eta \gg \eta_s$. Although Eq. (88) intends to be the upper limit, it is in practice close to the simulated response time from the full model with Eqs. (59), (60), (78), and (79) under the condition of Eq. (64) [2.8 ± 1.6% relative error (avg. ± s.d. in simulated conditions); $P < 10^{-4}$ and Text S2].

In parallel, the conventional approach to the response time with Eq. (82) can be taken too as above, except for the replacement of $\hat{\tau}_d$ by zero and the use of $\approx$ instead of $\gtrsim$ in Eq. (87). When $\eta \gg \eta_s$, the conventional response time up to $O(\eta_s/\eta)$ is given by

$$\ln\left(\frac{1}{1-\zeta}\right)\left[1-2(1-\sigma)\frac{\eta_s}{\eta}\right]. \quad (89)$$

This estimate tends to match the tQSSA model simulation with Eqs. (59) and (80) under the condition of Eq. (64) [2.8 ± 1.7% relative error (avg. ± s.d. in simulated conditions); $P < 10^{-4}$ and Text S2].

Subtracting Eq. (88) from Eq. (89) informs the lower limit of the difference between the conventional and our predictions, as follows:

$$2(1-\sigma)\left(\frac{1}{D_{\mathrm{TF}}}+\frac{1}{D}\right)\left[\ln\left(\frac{1}{1-\zeta}\right)-1-\frac{1}{D_{\mathrm{TF}}}-\frac{1}{D}\right]\frac{\eta_s}{\eta}. \quad (90)$$

As expected from the early discussion of Eq. (75), the minimum difference in Eq. (90) approaches zero when $D_{\mathrm{TF}}^{-1} + D^{-1} \to 0$. Consistent with Eq. (90), the tQSSA-to-full model difference in their simulated response times is linearly scaled to η_s/η ($R^2 > 0.87$) and its slope against η_s/η equals or exceeds that in Eq. (90) for most of the simulated conditions [88.8%; Fig. 6(e) and Text S2]. In the example of Fig. 6(e), the tQSSA model does overestimate the response time by about ten minutes and the error diminishes for larger η values. Lastly, note that the analytical expressions in Eqs. (88)–(90) are based on $\hat{\tau}$, and we thus divided them by $r_c + k_{\mathrm{dlt}}$ for actual response times.

E. Mammalian circadian clock

The quantitatively more accurate results from our revised MM rate law than from the previous approaches motivate us to ask the following question: can the revised MM rate law predict qualitatively new patterns of a dynamical system beyond its quantitative characterization? We will answer this question through the study of the mammalian circadian system.

The core part of the mammalian circadian clock harbors a transcriptional/post-translational negative feedback loop that generates autonomous protein oscillations with circadian rhythmicity [25,37]. Heterodimers of CLOCK and BMAL1 proteins activate the transcription of *Period* (*Per*) and *Cryptochrome* (*Cry*) genes, and the encoded PER and CRY proteins form PER–CRY complexes that are translocated to the nucleus. In the nucleus, they interact with CLOCK–BMAL1 complexes to inhibit the CLOCK–BMAL1 transcriptional activities. These positive (CLOCK and BMAL1) and negative (PER and CRY) arms constitute the negative feedback loop for circadian oscillations in protein levels and activities.

A previous study suggests that the tQSSA for the interaction between activator (CLOCK–BMAL1) and repressor (PER–CRY) leads to more natural rhythm generation than the sQSSA, because the tQSSA captures the ultrasensitive response of the repressor's transcription to the activator's or repressor's concentration—that is, a large change in the transcription rate from a small change in the activator or repressor level [18]. This ultrasensitive response, which is manifested by small K and balanced activator and repressor levels, amplifies rhythms and prevents their dampening [18,20]. Here, we will show that our revised MM rate law further captures the intrinsic time delays in the protein–protein and protein–DNA assembly formation and thereby predicts the rhythmic patterns not expected by the tQSSA.

For the modeling of the mammalian clock, we interpret $A(t)$, $B(t)$, and $C(t)$ in Eq. (1) as the concentrations of activator, repressor, and their complex in the nucleus, respectively. For simplicity, we assume the constancy of $A(t)$, i.e., $A(t) = A$ as the activator's oscillation is weaker than the repressor's and dispensable for the circadian rhythmicity [37–40]. The resulting model comprises Eq. (1) with $A(t) = A$ and the following equations modified from a previous model [18]:

$$\frac{\mathrm{d}M(t)}{\mathrm{d}t} = a_0 C_{\mathrm{TF}}(t) - b_0 M(t), \quad (91)$$

$$\frac{\mathrm{d}B_{\mathrm{cy}}(t)}{\mathrm{d}t} = a_1 M(t) - b_1 B_{\mathrm{cy}}(t), \quad (92)$$

$$\frac{\mathrm{d}B(t)}{\mathrm{d}t} = a_2 B_{\mathrm{cy}}(t) - r_{\mathrm{f}}[B(t) - C(t)] - r_{\mathrm{c}} C(t), \quad (93)$$

$$\frac{\mathrm{d}C_{\mathrm{TF}}(t)}{\mathrm{d}t} = \frac{k_{\mathrm{TFa}}}{V}[A - C(t)] - \{k_{\mathrm{TF}\delta} + k_{\mathrm{TFa}}[A - C(t)]\} C_{\mathrm{TF}}(t). \quad (94)$$

Here, $M(t)$, $B_{\mathrm{cy}}(t)$, and $C_{\mathrm{TF}}(t)$ are the concentrations of repressor mRNA, cytoplasmic repressor protein, and activator on repressor's promoter, respectively. Eq. (94) is equivalent to Eq. (30) in its content. a_0, a_1, and a_2 denote the transcription, translation, and translocation rates of the repressor, respectively. b_1 represents the sum of the translocation and degradation rates of the repressor in the cytoplasm, and thus satisfies $b_1 N_{\mathrm{c}} > a_2$ where N_{c} is the cytoplasm-to-nucleus volume ratio. b_0, r_{f}, and r_{c} are the degradation rates of repressor mRNA, free repressor protein, and activator-binding repressor protein, respectively. By definition, r_{c} satisfies $r_{\mathrm{c}} < k_{\delta}$ for k_{δ} in Eq. (1). k_{TFa}, $k_{\mathrm{TF}\delta}$, and V are the same as k_{a}, k_{δ}, and V in Eqs. (28)–(30), respectively. To be precise, $A - C(t)$ in Eq. (1) should be replaced by $A - C(t) - C_{\mathrm{TF}}(t)$; however, this replacement does not much affect our simulation results, and thus we keep the original form of Eq. (1) for the straightforward use of the approximants for $C(t)$ as will be demonstrated later.

Our model simulation with Eqs. (1) and (91)–(94) leads to the oscillation of the variables in a subset of the parameter conditions in Table S6 (Text S2). For comparison, we test another model with our revised MM rate law. This model consists only of Eqs. (91)–(93) where $C(t)$ and $C_{\mathrm{TF}}(t)$ are replaced by $C_{\gamma}(t)$ and $C_{\mathrm{TF}\gamma}(t)$ in Eqs. (19) and (40), respectively, and $A - C_{\gamma}(t)$ corresponds to $A_{\mathrm{TF}}(t)$, $k_{\mathrm{TF}\delta}$ to k_{δ}, and $k_{\mathrm{TF}\delta}/k_{\mathrm{TFa}}$ to K in Eqs. (32) and (40). Likewise, the tQSSA- and sQSSA-based models are constructed by using the approximants in Eqs. (7) and (9) instead of $C_{\gamma}(t)$, respectively, and using $C_{\mathrm{TFQ}}(t)$ in Eq. (32) instead of $C_{\mathrm{TF}\gamma}(t)$.

Consistent with the previous work and the characteristics of the well-studied Goodwin model [18,41], the sQSSA-based model fails to produce oscillations for any simulated conditions (Table S6 and Text S2). On the other hand, the tQSSA-based model generates oscillations as previously demonstrated [18], but with substantial deviations from the exact model simulation with Eqs. (1) and (91)–(94) (Fig. 7 and Text S2). For example, a decrease in $k_{\mathrm{TF}\delta}$ in the exact model simulation tends to facilitate the development of oscillations to some extent by widening the oscillatory range of $K_{\mathrm{TF}} \equiv k_{\mathrm{TF}\delta} k_{\mathrm{TFa}}^{-1}$, and concurrently lengthens the oscillation period [Figs. 7(a) and 7(c)]; the tQSSA-based model does not reproduce these patterns, though [Figs. 7(a) and 7(c)]. Besides, the exact simulation results exhibit the oscillations over the range of K far beyond small K values from the tQSSA-based results [Figs. 7(b) and 7(d)]. Moreover, the tQSSA-based oscillation periods are limited to short periods compared to the exact simulation results (Fig. 7).

In contrast, the simulation with our revised MM rate law shows good agreement with the exact model simulation in terms of the overall patterns of oscillation onset and periods (Fig. 7 and Text S2). For example, the revised MM rate law predicts the periods of 13.6 to 49.6 h with varying $k_{\mathrm{TF}\delta}$ at $K_{\mathrm{TF}} = 11.9$ nM in Fig. 7(a), and the exact periods span 13.0 to 33.4 h in the same conditions. Meanwhile, the tQSSA-based period is limited to 11.6 h there [Fig. 7(a)]. Regarding the revised rate law, the wide range of the oscillatory parameters and the period variations comparable to the exact simulation results comes from the time-delay terms in protein–protein and protein–DNA assembly formation in Eqs. (19) and (40). These intrinsic time-delay effects, which are absent in the tQSSA, enhance the rhythmicity of the dynamics and lengthen the oscillation periods. A caveat is that the revised rate law tends to rather overestimate the oscillatory parameter ranges compared to the exact model simulation (Fig. 7). Aside from this caveat, the revised rate law accounts for the overall qualitative and quantitative outcomes of the mammalian clock model not expected by the tQSSA or sQSSA.

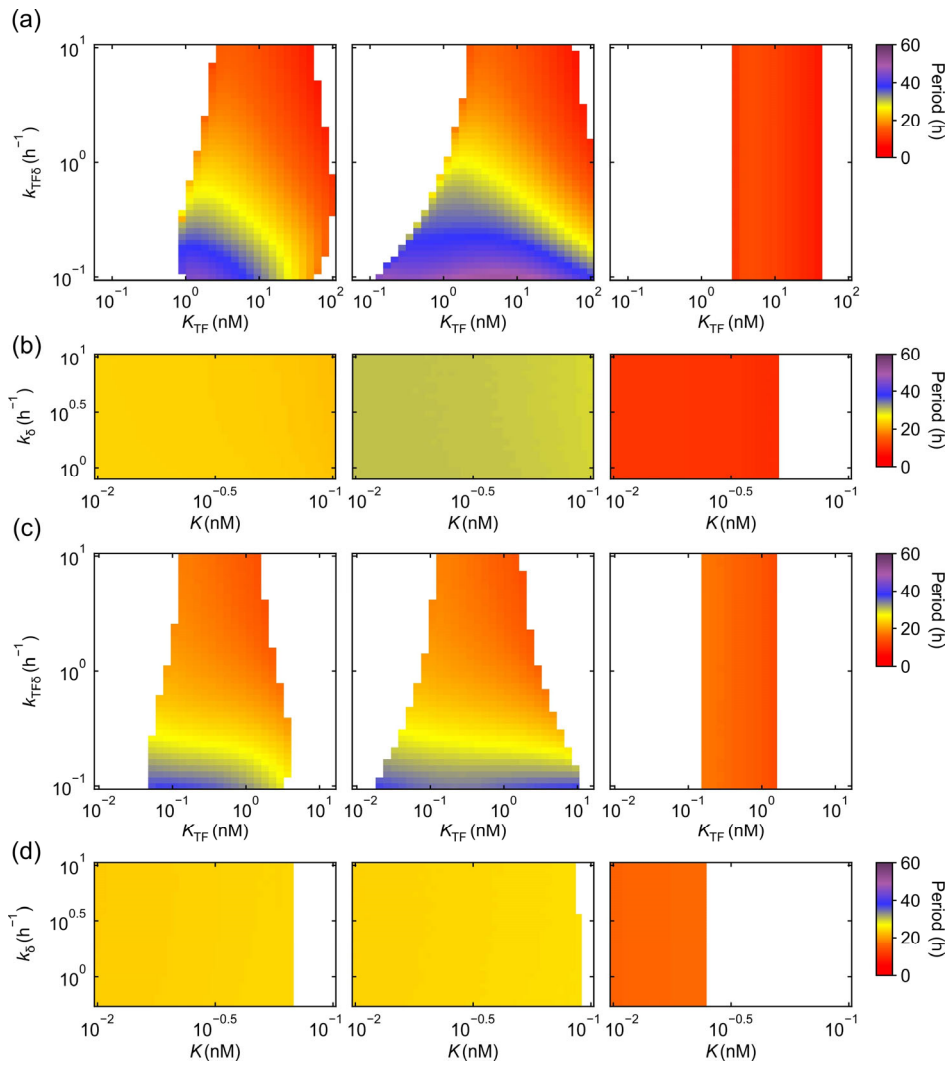

FIG. 7. Mammalian clock simulation with varying parameters. In (a)–(d), the parameter ranges with observed oscillations from each simulation scheme are colored by their oscillation periods, according to the color scale on the rightmost side. (a) and (b) have the same parameters except K_{TF} ($K_{\mathrm{TF}} \equiv k_{\mathrm{TF}\delta} k_{\mathrm{TFa}}^{-1}$), $k_{\mathrm{TF}\delta}$, K, and k_δ. Likewise, (c) and (d) have the same parameters except K_{TF}, $k_{\mathrm{TF}\delta}$, K, and k_δ. The simulation results from the full model with Eqs. (1) and (91)–(94) (left), from our revised MM rate law (center), and from the tQSSA (right) are presented over the ranges of K_{TF} and $k_{\mathrm{TF}\delta}$ in (a) and

(c), or the ranges of K and k_δ in (b) and (d), while the other parameters are fixed. For the simulation methods and parameters in (a)–(d), refer to Sec. III.E and Text S2.

F. Rhythmic degradation of proteins

According to previous reports, some circadian clock proteins are not only rhythmically produced but also decompose with rhythmic degradation rates [Figs. 8(a) and 8(b)] [42–46]. Recently, we have suggested that the rhythmic degradation rates of proteins with circadian production can spontaneously emerge without any explicitly time-dependent regulatory mechanism of the degradation processes [42,47]. If the rhythmic degradation rate peaks at the descending phase of the protein profile and stays relatively low elsewhere, it is supposed to save much of the biosynthetic cost in maintaining a circadian rhythm. A degradation mechanism with multiple post-translational modifications (PTMs), such as phospho-dependent ubiquitination, may elevate the rhythmicity of this degradation rate in favor of the biosynthetic cost saving [42,45]. Can our revised MM rate law explain this inherent rhythmicity in the degradation rates of circadian proteins?

In the following model, $A_0(t)$ and $A_1(t)$ represent the concentrations of unmodified and modified proteins, respectively, while the protein modified by ubiquitination undergoes degradation. The protein turnover dynamics is described by

$$\frac{\mathrm{d}A_0(t)}{\mathrm{d}t} = g(t) - a_0 A_0(t), \qquad (95)$$

$$\frac{\mathrm{d}A_1(t)}{\mathrm{d}t} = a_0 A_0(t) - r_\mathrm{c} A_1(t), \qquad (96)$$

where $g(t)$ and a_0 are the protein synthesis (translation) and modification rates, respectively, and r_c is the modified protein's turnover rate. If the protein turnover requires multiple preceding PTMs such as polyubiquitination and mono- or multisite phosphorylation with subsequent ubiquitination, we consider Eq. (95) and the following equation instead of Eq. (96):

$$\frac{\mathrm{d}A_i(t)}{\mathrm{d}t} = a_{i-1} A_{i-1}(t) - a_i A_i(t), \qquad (97)$$

where $A_i(t)$ denotes the concentration of the i-th modified protein with $i = 1, 2, \cdots, n$ (n is the total number of the PTMs), a_i for $i \leq n-1$ denotes the rate of the ($i+1$)-th modification, and $a_n \equiv r_\mathrm{c}$, the turnover rate of the n-th modified protein. In the case of $n = 1$, Eq. (97) becomes the same as Eq. (96). Therefore, unless specified, we will consider Eqs. (95) and (97) whether $n = 1$ or $n > 1$.

For the total protein concentration $A(t) \equiv \sum_{i=0}^{n} A_i(t)$, Eqs. (95) and (97) result in

$$\frac{\mathrm{d}A(t)}{\mathrm{d}t} = g(t) - r(t)A(t), \qquad (98)$$

where $r(t)$ is the protein degradation rate given by

$$r(t) = r_\mathrm{c} \frac{A_n(t)}{A(t)}. \qquad (99)$$

To exclude the possibility of the time-dependent regulation of the degradation process, a_i's with $0 \leq i \leq n$ in Eqs. (95) and (97) are constants. Given the circadian profile of protein synthesis rate $g(t)$, the numerical solution of Eqs. (95), (97), and (99) gives rise to the degradation rate $r(t)$ (Text S2). In this calculation, we use the sinusoidal form of $g(t)$:

$$g(t) = g_\mathrm{max} \left\{ 1 - \frac{\alpha_\mathrm{g}}{2} \left[1 + \cos\left(\frac{2\pi t}{T} \right) \right] \right\}, \qquad (100)$$

where g_max, α_g, and T are constants.

On the other hand, our revised MM rate law provides the analytical estimate of $r(t)$ through the comparison of seemingly unrelated but mathematically equivalent systems. Because the periodic $g(t)$ assures $\langle A_i'(t) \rangle = \langle A_i(t) \rangle' = 0$ ($\langle \cdot \rangle$ is a time average), $\langle g(t) \rangle = a_i \langle A_i(t) \rangle$ and $\langle A_i(t) \rangle$ is then inversely proportional to a_i. Hence, $A(t) \approx A_u(t) + A_v(t)$ for $i = u, v$ ($u < v$) that hold the two smallest a_i values among all a_i's. In addition, a_i's are larger for $i \neq u, v$ by definition and therefore the corresponding $A_i(t)$'s are likely to follow $A_i'(t) \approx 0$ with the effect of $-a_i A_i(t)$ in Eq. (97). Subsequently, $a_v A_v(t) \approx a_{v+1} A_{v+1}(t) \approx \cdots \approx r_\mathrm{c} A_n(t)$. As a result, Eqs. (97) and (99) reduce to

$$\frac{\mathrm{d}A_v(t)}{\mathrm{d}t} \approx \sum_{i=u+1}^{v} \frac{\mathrm{d}A_i(t)}{\mathrm{d}t} = a_u A_u(t) - a_v A_v(t)$$
$$\approx a_u[A(t) - A_v(t)] - a_v A_v(t), \quad (101)$$
$$r(t) \approx a_v \frac{A_v(t)}{A(t)}. \quad (102)$$

When $n = 1$, it is obvious that $u = 0$, $v = 1$, and symbol $=$ replaces $\approx$ in Eqs. (101) and (102). Eqs. (101) and (102) may not satisfactorily work for large n due to accumulating errors in the approximation, but still capture the core structure of the dynamics. We then observe the mathematical equivalence of Eqs. (30) and (101) despite their different biological contexts: $C_{\mathrm{TF}}(t)$ and $A_v(t)$, V^{-1} ($= B_{\mathrm{DNA}}$) and $A(t)$, $k_{\mathrm{a}}A_{\mathrm{TF}}(t)$ and a_u, and k_δ and a_v in correspondence. Using this correspondence and Eqs. (32), (40), and (102), we estimate $r(t)$ as

$$r_\gamma(t) \equiv \frac{a_v}{A(t)} \min\left[\frac{a_u}{a_u+a_v} A\left(t - \frac{1}{a_u+a_v}\right), A(t)\right] \text{ and } r_{\mathrm{Q}}(t) \equiv \frac{a_u a_v}{a_u+a_v}, \quad (103)$$

where the former is based on our revised MM rate law in Eq. (40) and condition $A_v(t) \leq A(t)$, and the latter on the conventional scheme in Eq. (32). In the case of the latter, the distinction between the tQSSA and sQSSA is meaningless, as mentioned earlier.

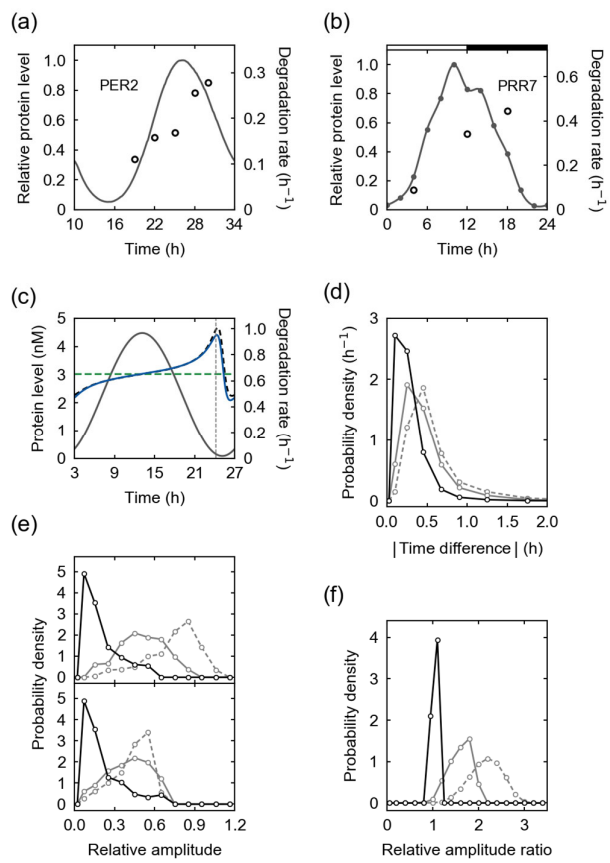

FIG. 8. Rhythmic degradation of circadian proteins. (a) The experimental abundance levels (solid line) and degradation rates (open circles) of the mouse PERIOD2 (PER2) protein [43]. (b) The experimental abundance levels (dots, interpolated by a solid line) and degradation rates (open circles) of PSEUDO RESPONSE REGULATOR 7 (PRR7) protein in *Arabidopsis* [44,45,54]. Horizontal white and black segments correspond to light and dark intervals, respectively. (c) Simulated protein abundance $A(t)$ (gray solid line) and degradation rate $r(t)$ (black dashed line), along with the approximate degradation rates $r_\gamma(t)$ (blue solid line) and $r_{\mathrm{Q}}(t)$ (green dashed line) from Eqs. (95), (97), (99), (100), and (103) when $n = 1$. $r_{\gamma 2}(t)$ in Eq. (104) highly overlaps with $r_\gamma(t)$ and is thus omitted here. A vertical dashed line

corresponds to the peak time of $-A'(t)/A(t)$. (d) The probability distribution of the peak-time difference between $r(t)$ and $-A'(t)/A(t)$ over randomly-sampled parameter sets in Table S7, when $n = 1$ (black solid line), $n = 2$ (gray solid line), or $n = 3$ (gray dashed line). (e) The probability distribution of $r(t)$'s relative amplitude (top) or its estimate in Eq. (105) (bottom) with a given profile of $A(t)$ over randomly-sampled parameter sets in Table S7, when $n = 1$ (black solid line), $n = 2$ (gray solid line), or $n = 3$ (gray dashed line). Regarding the profile of $A(t)$, its relative amplitude is set to 1. (f) The probability distribution of the ratio of $r(t)$'s relative amplitude to its estimate in Eq. (105) over randomly-sampled parameter sets in Table S7, when $n = 1$ (black solid line), $n = 2$ (gray solid line), or $n = 3$ (gray dashed line). For the detailed methods in (a)–(f), refer to Text S2.

Our revised rate law naturally accounts for the rhythmicity in experimental degradation rates through the inherent time delay in protein modification and turnover. To clarify it, we simplify $r_\gamma(t)$ in Eq. (103) as

$$r_\gamma(t) \approx r_{\gamma 2}(t) \equiv \frac{a_u a_v}{a_u+a_v}\frac{A\left(t-\frac{1}{a_u+a_v}\right)}{A(t)} = \frac{a_u a_v}{a_u+a_v}\left\{1-\frac{1}{a_u+a_v}\left[\frac{1}{A(t)}\frac{\mathrm{d}A(t)}{\mathrm{d}t}\right]+\cdots\right\}. \quad (104)$$

The above $r_{\gamma 2}(t)$ is an approximately increasing function of $-A'(t)/A(t)$ and thus predicts that the degradation rate would increase as time goes from the ascending to descending phases of a protein profile, as experimentally observed in Figs. 8(a) and 8(b). In contrast, the conventional scheme does not predict a rhythmic degradation rate, as $r_{\mathrm{Q}}(t)$ in Eq. (103) is constant over time. The rhythmicity from our result can be explained by an unsynchronized interplay between protein translation and degradation processes [42] due to their inter-event time delay. For example, in the case of protein ubiquitination, E3 ubiquitin ligases with a finite binding affinity would not always capture all newly-translated substrates, and therefore, a lower proportion of the substrates may be ubiquitinated during the ascending phase of the substrate profile than during the descending phase. The degradation rate hence tends to be lower at times other than the descending phase. Additional PTMs like phosphorylation, if required for the ubiquitination, can even possibly retard the full substrate modification and thereby increase the degradation rhythmicity for a given substrate profile. One may expect that these effects would be enhanced with more limited ubiquitin ligases or kinases, under the condition when the substrate level with circadian production undergoes a steeply rising and falling oscillation. This expectation is supported by the relative amplitude of the degradation rate estimated by Eq. (104):

$$\frac{\max_t[r(t)]-\min_t[r(t)]}{\langle r(t)\rangle} \sim \frac{1}{a_u+a_v}\left\{\max_t\left[\frac{1}{A(t)}\frac{\mathrm{d}A(t)}{\mathrm{d}t}\right]-\min_t\left[\frac{1}{A(t)}\frac{\mathrm{d}A(t)}{\mathrm{d}t}\right]\right\}, \quad (105)$$

where $\langle\cdot\rangle$ is a time average. The relative amplitude of $r(t)$ here is roughly proportional to $(a_u + a_v)^{-1}$ as well as to the amplitude of $A'(t)/A(t)$. Multiple PTMs with the same profile of $A(t)$ can enhance this degradation rhythmicity because $n \geq 2$ invites the possibility of smaller a_u and a_v values than expected for $n = 1$. Eq. (104) further predicts that the degradation rate would peak around the peak time of $-A'(t)/A(t)$.

In the example of Fig. 8(c), the degradation rate $r(t)$ computed fully from Eqs. (95), (97), (99), and (100) when $n = 1$ does exhibit the rhythmic profile in excellent agreement with our prediction [$r_\gamma(t)$ in Eq. (103)], not the conventional one [$r_{\mathrm{Q}}(t)$ in Eq. (103)]. Notably, the peak time of $r(t)$ there is very close to that of $-A'(t)/A(t)$ as predicted in Eq. (104). Indeed, the peaks of $r(t)$ profiles show only < 1h time differences from the maximum $-A'(t)/A(t)$ values across most (89–99%) of the simulated conditions of $n = 1$ to 3 [Fig. 8(d); Table S7 and Text S2]. In addition, for each $A(t)$ profile, $r(t)$ tends to become more rhythmic and have a larger relative amplitude as n increases from 1 [Fig. 8(e)], supporting the above argument that multiple PTMs can facilitate degradation rhythmicity [42]. The approximate relative amplitude in Eq. (105) shows such a tendency for $n = 1, 2$ too, yet not clearly for $n = 3$ unlike the correctly-calculated relative amplitude [Fig. 8(e)]. This inaccuracy with $n = 3$ comes from the accumulated errors over n in the approximation in Eqs. (101) and (102), as we foresaw above. Still, the estimate in Eq. (105) accounts for at least the order of magnitude of the actual relative amplitude with $n > 1$ while strikingly accurate for $n = 1$, as the ratio of the actual to

estimated one almost equals 1 at $n = 1$ and remains to be $O(1)$ at $n = 2, 3$ [Fig. 8(f)]. Moreover, the estimated and actual values considerably correlate at each n, even $n = 3$ (Spearman's $\rho = 0.49$ and $P < 10^{-4}$; Text S2).

Together, our revised MM rate law provides a useful analytical framework of the rhythmic degradation of circadian proteins, which is hardly explained by the conventional means.

IV. PARAMETER ESTIMATION

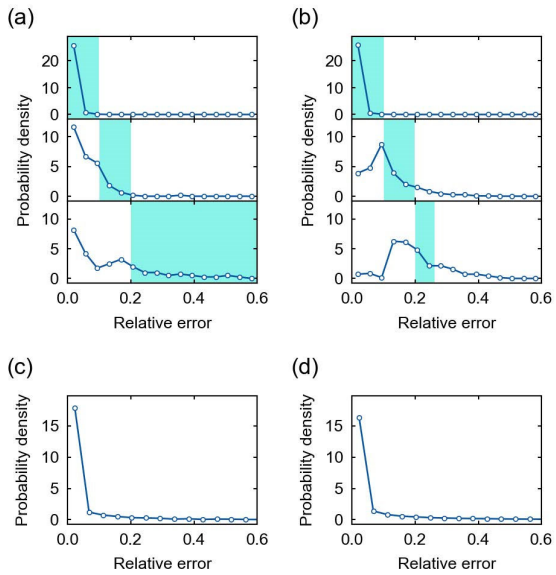

FIG. 9. Parameter estimation for protein–protein and TF–DNA interaction models. (a) The probability distribution of the relative error of estimated K for a protein–protein interaction model in Eqs. (1) and (49). The estimation was performed by the fitting of $C_\gamma(t)$ [Eq. (19)] to $C(t)$ [Eq. (1)], when the relative error of the estimated K from $C_{\mathrm{tQ}}(t)$ [Eq. (7)] is < 0.1 (top), ≥ 0.1 and < 0.2 (center), or ≥ 0.2 (bottom). (b) The probability distribution of the relative error of estimated K for a TF–DNA interaction model in Eqs. (30) and (52). The estimation was performed by the fitting of $C_{\mathrm{TF}\gamma}(t)$ [Eq. (40)] to $C_{\mathrm{TF}}(t)$ [Eq. (30)], when the relative error of the estimated K from $C_{\mathrm{TFQ}}(t)$ [Eq. (32)] is < 0.1 (top), ≥ 0.1 and < 0.2 (center), or ≥ 0.2 (bottom). In (a) and (b), shaded is the actually-observed range of the relative error of the estimated K from $C_{\mathrm{tQ}}(t)$ (a) or $C_{\mathrm{TFQ}}(t)$ (b) across our simulated conditions (Text S2). More than a half of the simulated conditions show that the relative error of the estimated K from $C_\gamma(t)$ (a) or $C_{\mathrm{TF}\gamma}(t)$ (b) is < 0.1 (top and center) or < 0.2 (bottom). (c) The probability distribution of the relative error of k_δ estimated by $C_\gamma(t)$ for the protein–protein interaction model used in (a). (d) The probability distribution of the relative error of k_δ estimated by $C_{\mathrm{TF}\gamma}(t)$ for the TF–DNA interaction model used in (b). Although not shown in (c) and (d), there exist a negligible portion of the simulated conditions where the relative error of the estimated k_δ is > 0.6. For the detailed methods in (a)–(d), refer to Text S2.

An accurate function of variables and parameters is required for good parameter estimation based on the fitting of the function [13,48,49]. In this regard, we compare the accuracies of parameters estimated from our revised MM rate law and the tQSSA by their fitting to the full model simulation results. Specifically, we consider protein–protein interactions with time-varying protein concentrations $A(t)$ and $B(t)$ from Eq. (49) by $A(t) = K\overline{A}(\tau)$, $B(t) = K\overline{B}(\tau)$, $t = k_\delta^{-1}\tau$, and parameters set as in Text S2. Given these profiles $A(t)$ and $B(t)$ and the parameters K and k_δ, $C(t)$ is determined by Eq. (1) and we treat this $C(t)$ as the "true" concentration of protein complex. To the profile of $C(t)$, we then fit our revised MM rate law [$C_\gamma(t)$ in Eq. (19)] or the tQSSA [$C_{\mathrm{tQ}}(t)$ in Eq. (7)] based on the given $A(t)$ and $B(t)$, and

estimate the original parameters of $C(t)$: the fitting of $C_\gamma(t)$ estimates both K and k_δ, and the fitting of $C_{\mathrm{tQ}}(t)$ estimates only K (Text S2). Because the tQSSA has already been reported for its better parameter-estimation capability than the sQSSA's [12,49], we here do not evaluate the case of the sQSSA. In this work, the parameters were estimated by Powell's method [50], and an alternative method hardly changed our results (Text S2).

Likewise, we consider TF–DNA interactions with time-varying TF concentration $A_{\mathrm{TF}}(t)$ from Eq. (52) by $A_{\mathrm{TF}}(t) = K\overline{A}_{\mathrm{TF}}(\tau)$, $t = k_\delta^{-1}\tau$, and parameters set as in Text S2. Given the profile $A_{\mathrm{TF}}(t)$, B_{DNA} $(= V^{-1})$, and the kinetic parameters K and k_δ, $C_{\mathrm{TF}}(t)$ is determined by Eq. (30) and we treat this $C_{\mathrm{TF}}(t)$ as the "true" concentration of TF–DNA assembly. To the profile of $C_{\mathrm{TF}}(t)$, we then fit $C_{\mathrm{TF}\gamma}(t)$ in Eq. (40) and $C_{\mathrm{TFQ}}(t)$ in Eq. (32) based on the given $A_{\mathrm{TF}}(t)$ and V^{-1}, and estimate the original parameters of $C_{\mathrm{TF}}(t)$: the fitting of $C_{\mathrm{TF}\gamma}(t)$ estimates both K and k_δ, and the fitting of $C_{\mathrm{TFQ}}(t)$ estimates only K (Text S2). Like the above protein–protein interaction case, we used Powell's method to estimate the parameters [50], while an alternative method did not much affect our results (Text S2).

In the case of protein–protein interactions, Fig. 9(a) reveals that the use of our revised rate law improves parameter estimation compared to the tQSSA, as $C_\gamma(t)$ tends to give a more accurate estimate of K than $C_{\mathrm{tQ}}(t)$. For example, in the cases that the relative error of K estimated from $C_{\mathrm{tQ}}(t)$ is ≥ 0.2, most of the $C_\gamma(t)$-based estimates (75.9%) show the relative error < 0.2 ($P < 10^{-4}$ and Text S2), and even their 65.9% show the relative error < 0.1 [Fig. 9(a)]. In the case of TF–DNA interactions, our revised MM rate law allows a comparably weak improvement in the estimation of K, though [Fig. 9(b)].

Unlike K, k_δ can only be estimated through $C_\gamma(t)$ and $C_{\mathrm{TF}\gamma}(t)$, and hence the comparison to its estimates from $C_{\mathrm{tQ}}(t)$ and $C_{\mathrm{TFQ}}(t)$ is not possible. Of note, k_δ is found to have the relative error < 0.1 for most of the $C_\gamma(t)$- and $C_{\mathrm{TF}\gamma}(t)$-based estimates, 86.6% and 80.7%, respectively [Figs. 9(c) and 9(d)].

V. CONCLUSION AND DISCUSSION

In this study, we proposed the revised MM rate law, which improves the description of molecular interaction dynamics with time-varying molecular concentrations. When applied to protein–protein and TF–DNA interaction dynamics, our revised MM rate law tends to capture the correct phases of the oscillatory profiles, compared to the existing rate laws. The revised rate law also improves the relevant parameter estimation. In the case of the mammalian circadian clock, the revised rate law well accounts for the overall patterns of oscillation onsets and periods from the full model simulations, which are not captured by the tQSSA or sQSSA. Notwithstanding the apparent complexity of our revised rate law, it provides invaluable analytical insights into the response times of autoregulated genetic circuits and the spontaneous establishment of the rhythmic degradation rates of circadian proteins. This demonstrated utility of our revised MM rate law for various systems in transient or oscillatory states originates from the rigorously derived, time-delay effects in the molecular complex formation. Our approach enhances the mathematical understanding of the time-varying behaviors of complex-complete mass-action models [36,42,51] beyond only their steady states.

Further elaboration and physical interpretation of our theoretical framework, in concert with extensive experimental profiling of molecular complexes in regulatory or signaling pathways [15,16,31–33], are warranted for the correct understanding and modeling of the interplay between cellular components and its functional consequences. Although the mammalian and plant data presented here are supportive of our theoretical predictions, experimental tests are clearly warranted including direct validation of the proposed rate law. This validation could involve the measurement of the time series of molecular complex concentrations by co-immunoprecipitation assays or other techniques, and high temporal resolution data are

preferred for the comparison with the proposed rate law. Besides, comprehensive consideration of stochastic fluctuation and nonlinearity in molecular binding events [29,52,53] would be needed for more complete development of our theory, although the stochasticity in TF–DNA interactions is partially reflected in this work.

ACKNOWLEDGMENTS

We thank Haneul Kim for useful discussions.

REFERENCES

1. V. Henri, *Lois Générales de l'Action des Diastases* (Librairie Scientifique A. Hermann, 1903).
2. L. Michaelis and M. L. Menten, *Die Kinetik der Invertinwirkung*, Biochem. Z. **49**, 333–369 (1913).
3. G. E. Briggs and J. B. S. Haldane, *A Note on the Kinetics of Enzyme Action*, Biochem. J. **19**, 338 (1925).
4. J. Gunawardena, *Time-Scale Separation–Michaelis and Menten's Old Idea, Still Bearing Fruit*, FEBS. J. **281**, 473–488 (2014).
5. C. Gérard and A. Goldbeter, *A Skeleton Model for the Network of Cyclin-Dependent Kinases Driving the Mammalian Cell Cycle*, Interface Focus **1**, 24–35 (2011).
6. K. C. Chen, A. Csikasz-Nagy, B. Gyorffy, J. Val, B. Novak, and J. J. Tyson, *Kinetic Analysis of a Molecular Model of the Budding Yeast Cell Cycle*, Mol. Biol. Cell **11**, 369–391 (2000).
7. J. C. Leloup and A. Goldbeter, *Toward a Detailed Computational Model for the Mammalian Circadian Clock*, Proc. Natl. Acad. Sci. USA **100**, 7051–7056 (2003).
8. J. Garcia-Ojalvo, *Modeling Gene Expression in Time and Space*, Annu. Rev. Biophys. **42**, 605–627 (2013).
9. M. Foo, D. E. Somers, and P.-J. Kim, *Kernel Architecture of the Genetic Circuitry of the Arabidopsis Circadian System*, PLoS Comput. Biol. **12**, e1004748 (2016).
10. T. D. Pollard, *A Guide to Simple and Informative Binding Assays*, Mol. Biol. Cell **21**, 4061–4067 (2010).
11. A. D. Attie and R. T. Raines, *Analysis of Receptor–Ligand Interactions*, J. Chem. Educ. **72**, 119 (1995).
12. J. K. Kim and J. J. Tyson, *Misuse of the Michaelis–Menten Rate Law for Protein Interaction Networks and Its Remedy*, PLoS Comput. Biol. **16**, e1008258 (2020).
13. S. Schnell and P. K. Maini, *A Century of Enzyme Kinetics: Reliability of the K_M and v_{max} Estimates*, Comm. Theor. Biol. **8**, 169–187 (2003).
14. L. A. Segel and M. Slemrod, *The Quasi-Steady-State Assumption: a Case Study in Perturbation*, SIAM Rev. **31**, 446–477 (1989).
15. A. Fujioka, K. Terai, R. E. Itoh, K. Aoki, T. Nakamura, S. Kuroda *et al.*, *Dynamics of the Ras/ERK MAPK Cascade as Monitored by Fluorescent Probes*, J. Biol. Chem. **281**, 8917–8926 (2006).
16. N. Blu¨thgen, F. J. Bruggeman, S. Legewie, H. Herzel, H. V. Westerhoff, and B. N. Kholodenko, *Effects of Sequestration on Signal Transduction Cascades*, FEBS J. **273**, 895–906 (2006).
17. S. Carmi, E. Y. Levanon, S. Havlin, and E. Eisenberg, *Connectivity and Expression in Protein Networks: Proteins in a Complex Are Uniformly Expressed*, Phys. Rev. E. **73**, 031909 (2006).
18. J. K. Kim and D. B. Forger, *A Mechanism for Robust Circadian Timekeeping via Stoichiometric Balance*, Mol. Syst. Biol. **8**, 630 (2012).

19. A. M. Bersani, E. Bersani, G. Dell'Acqua, and M. G. Pedersen, *New Trends and Perspectives in Nonlinear Intracellular Dynamics: One Century from Michaelis–Menten Paper*, Contin. Mech. Thermodyn. **27**, 659–684 (2015).
20. N. E. Buchler and M. Louis, *Molecular Titration and Ultrasensitivity in Regulatory Networks*, J. Mol. Biol. **384**, 1106–1119 (2008).
21. A. R. Tzafriri, *Michaelis–Menten Kinetics at High Enzyme Concentrations*, Bull. Math. Biol. **65**, 1111–1129 (2003).
22. H. C. Lim, *On Kinetic Behavior at High Enzyme Concentrations*, AICHE J. **19**, 659–661 (1973).
23. S. Cha, *Kinetic Behavior at High Enzyme Concentrations: Magnitude of Errors of Michaelis–Menten and Other Approximations*, J. Biol. Chem. **245**, 4814–4818 (1970).
24. K. J. Laidler, *Theory of the Transient Phase in Kinetics, with Special Reference to Enzyme Systems*, Can. J. Chem. **33**, 1614–1624 (1955).
25. F. Gachon, E. Nagoshi, S. Brown, J. Ripperger, and U. Schibler, *The Mammalian Circadian Timing System: From Gene Expression to Physiology*, Chromosoma **113**, 103–112 (2004).
26. D. H. Nagel and S. A. Kay, *Complexity in the Wiring and Regulation of Plant Circadian Networks*, Curr. Biol. **22**, R648–R657 (2012).
27. T. S. Hatakeyama and K. Kaneko, *Reciprocity between Robustness of Period and Plasticity of Phase in Biological Clocks*, Phys. Rev. Lett. **115**, 218101 (2015).
28. N. Mosheiff, B. M. C. Martins, S. Pearl-Mizrahi, A. Grünberger, S. Helfrich, I. Mihalcescu, D. Kohlheyer, J. C. W. Locke, L. Glass, and N. Q. Balaban, *Inheritance of Cell-Cycle Duration in the Presence of Periodic Forcing*, Phys. Rev. X **8**, 021035 (2018).
29. V. Kampen and N. Godfried, *Stochastic Processes in Physics and Chemistry* (Elsevier, 1992).
30. E. Levine and T. Hwa, *Stochastic Fluctuations in Metabolic Pathways*, Proc. Natl. Acad. Sci. USA **104**, 9224–9229 (2007).
31. W.-Y. Kim, S. Fujiwara, S.-S. Suh, J. Kim, Y. Kim, L. Han *et al*., *ZEITLUPE is a Circadian Photoreceptor Stabilized by GIGANTEA in Blue Light*, Nature **449**, 356–360 (2007).
32. J. Y. Cha, J. Kim, T.-S. Kim, Q. Zeng, L. Wang, S. Y. Lee, W.-Y. Kim, and D. E. Somers, *GIGANTEA Is a Co-Chaperone Which Facilitates Maturation of ZEITLUPE in the Arabidopsis Circadian Clock*, Nat. Commun. **8**, 3 (2017).
33. C.-M. Lee, M.-W. Li, A. Feke, W. Liu, A. M. Saffer, and J. M. Gendron, *GIGANTEA Recruits the UBP12 and UBP13 Deubiquitylases to Regulate Accumulation of the ZTL Photoreceptor Complex*, Nat. Commun. **10**, 3750 (2019).
34. Y. T. Maeda and M. Sano, *Regulatory Dynamics of Synthetic Gene Networks with Positive Feedback*, J. Mol. Biol. **359**, 1107–1124 (2006).
35. N. Rosenfeld, M. B. Elowitz, and U. Alon, *Negative Autoregulation Speeds the Response Times of Transcription Networks*, J. Mol. Biol. **323**, 785–793 (2002).
36. C. Jeynes-Smith and R. P. Araujo, *Ultrasensitivity and Bistability in Covalent-Modification Cycles with Positive Autoregulation*, Proc. R. Soc. A **477**, 20210069 (2021).
37. C. Lee, J. P. Etchegaray, F. R. Cagampang, A. S. Loudon, and S. M. Reppert, *Posttranslational Mechanisms Regulate the Mammalian Circadian Clock*, Cell **107**, 855–867 (2001).
38. A. C. Liu *et al*., *Redundant Function of REV-ERBα and β and Non-Essential Role for Bmal1 Cycling in Transcriptional Regulation of Intracellular Circadian Rhythms*, PLoS Genet. **4**, e1000023 (2008).
39. N. Preitner *et al*., *The Orphan Nuclear Receptor REV-ERBα Controls Circadian Transcription within the Positive Limb of the Mammalian Circadian Oscillator*, Cell **110**, 251–260 (2002).
40. E. L. McDearmon *et al*., *Dissecting the Functions of the Mammalian Clock Protein BMAL1 by Tissue-Specific Rescue in Mice*, Science **314**, 1304–1308 (2006).

41. B. C. Goodwin, *Oscillatory Behavior in Enzymatic Control Processes*, Adv. Enzyme Regul. **3**, 425–438 (1965).
42. R. Lim, J. Chae, D. E. Somers, C.-M. Ghim, and P.-J. Kim, *Cost-Effective Circadian Mechanism: Rhythmic Degradation of Circadian Proteins Spontaneously Emerges without Rhythmic Post-Translational Regulation*, iScience **24**, 102726 (2021).
43. M. Zhou, J. K. Kim, G. W. Eng, D. B. Forger, and D. M. Virshup, *A Period2 Phosphoswitch Regulates and Temperature Compensates Circadian Period*, Mol. Cell **60**, 77–88 (2015).
44. E. M. Farre´ and S. A. Kay, *PRR7 Protein Levels Are Regulated by Light and the Circadian Clock in Arabidopsis*, Plant J. **52**, 548–560 (2007).
45. H.-H. Jo, Y. J. Kim, J. K. Kim, M. Foo, D. E. Somers, and P.-J. Kim, *Waveforms of Molecular Oscillations Reveal Circadian Timekeeping Mechanisms*, Commun. Biol. **1**, 207 (2018).
46. G. van Ooijen, L. E. Dixon, C. Troein, and A. J. Millar, *Proteasome Function Is Required for Biological Timing throughout the Twenty-Four Hour Cycle*, Curr. Biol. **21**, 869–875 (2011).
47. J. Chae, R. Lim, C.-M. Ghim, and P.-J. Kim, *Backward Simulation for Inferring Hidden Biomolecular Kinetic Profiles*, STAR Protoc. **2**, 100958 (2021).
48. W. Stroberg and S. Schnell, *On the Estimation Errors of K_M and V from Time-Course Experiments Using the Michaelis–Menten Equation*, Biophys. Chem. **219**, 17 (2016).
49. B. Choi, G. A. Rempala, and J. K. Kim, *Beyond the Michaelis–Menten Equation: Accurate and Efficient Estimation of Enzyme Kinetic Parameters*, Sci. Rep. **7**, 1–11 (2017).
50. M. J. D. Powell, *An Efficient Method for Finding the Minimum of a Function of Several Variables without Calculating Derivatives*, Comput. J. **7**, 155–162 (1964).
51. A. K. Manrai and J. Gunawardena, *The Geometry of Multisite Phosphorylation*, Biophys. J. **95**, 5533–5543 (2008).
52. C.-M. Ghim and E. Almaas, *Two-Component Genetic Switch as a Synthetic Module with Tunable Stability*, Phys. Rev. Lett. **103**, 028101 (2009).
53. P.-J. Kim and N. D. Price, *Macroscopic Kinetic Effect of Cell-to-Cell Variation in Biochemical Reactions*, Phys. Rev. Lett. **104**, 148103 (2010).
54. N. Nakamichi *et al*., *PSEUDO-RESPONSE REGULATORS 9, 7, and 5 Are Transcriptional Repressors in the Arabidopsis Circadian Clock*, Plant Cell **22**, 594–605 (2010).